Suspended Sediment Drift and Dispersion at Hibernia

T. Tedford, A. Drozdowski and C.G. Hannah

Ocean Sciences Division
Maritimes Region
Fisheries and Oceans Canada

Bedford Institute of Oceanography
P.O. Box 1006
Dartmouth, Nova Scotia
Canada B2Y 4A2

2003

Canadian Technical Report of Hydrography and Ocean Sciences 227

Fisheries and Oceans Canada | Pêches et Océans Canada

Canada

103-03416/

Canadian Technical Report of
Hydrography and Ocean Sciences 227

2003

Suspended Sediment Drift and Dispersion at Hibernia

by

T. Tedford, A. Drozdowski and C.G. Hannah

Ocean Sciences Division
Maritimes Region
Fisheries and Oceans Canada

Bedford Institute of Oceanography
P.O. Box 1006
Dartmouth, N.S.
Canada B2Y 4A2

©Her Majesty the Queen in Right of Canada 2003
Cat. No. Fs 97-18/227E ISSN 0711-6764

Correct citation for this publication:

Tedford, T., A. Drozdowski and C.G. Hannah, 2003. Suspended Sediment Drift and Dispersion at Hibernia. Can. Tech. Rep. Hydrogr. Ocean Sci. 227: vi+57 p.

Contents

Abstract/Résumé vi

1 Introduction 1

2 Model Inputs 2
- 2.1 Currents and Waves . . . 2
- 2.2 Settling Velocity . . . 6
- 2.3 Friction Velocity . . . 8
- 2.4 Maximum Sediment Profile Height . . . 11
- 2.5 Drill Mud Input . . . 18
- 2.6 Other Input Parameters . . . 19

3 Model Output 20
- 3.1 Derived Quantities . . . 20
- 3.2 Median Height . . . 21
- 3.3 Scaling Parameters and Near-Bottom Concentrations . . . 21

4 Median Sediment Height 21

5 Sensitivity Analysis 28

6 Drift and Dispersion at Hibernia 35
- 6.1 Fixed Settling Velocity . . . 35
- 6.2 Variable Settling Velocity . . . 47

7 Discussion and Summary 50

References 54

A Alternative Maximum Sediment Height Profiles 56

List of Figures

1 Hibernia location map 2
2 Schematic of inputs, outputs and processes. 3
3 Current magnitude at 3 and 10 meters above bottom. 4
4 Significant wave height and period. 5
5 Progressive vector diagram for the two moored current meters 6
6 Velocity profile constructed using exponential decay 7
7 Illustration of sediment breakup and flocculation 9
8 Difference between total friction velocity and skin friction velocity 11
9 Hourly friction velocity for u_{*g}, u_{*c} and u_{*cw}. 12
10 Monthly friction velocity statistics for u_{*g}, u_{*c} and u_{*cw}. 13
11 Seasonal climatology for u_{*g}, u_{*c} and u_{*cw}. 14
12 Density profiles observed at Hibernia during the period of interest. 15
13 Seasonal density profiles in the vicinity of Hibernia 16
14 Time series of seasonally varying h_{max} 18
15 The hourly median height of sediment particles with h_{max} = 84 m. 23
16 The hourly median height of sediment particles with variable h_{max}. 24
17 The hourly median height of sediment particles with h_{max} = 20 m. 25
18 Monthly median height for u_{*cw} and h_{max} = 84m. 26
19 Difference between the total and skin friction median height. 28
20 Five day averages of u_{*c} for the period of the sensitivity analysis. 29
21 Velocity of the horizontal centre of mass for the lighter sediment 30
22 Velocity of the horizontal centre of mass for the heavier sediment 31
23 Five day averaged horizontal diffusivity for the lighter sediment. 33
24 Five day averaged horizontal diffusivity for the heavier sediment. 34
25 Time series of five day averaged drift 37
26 Scatter plot of five day averaged drift 38
27 Log-polar drift plot 43
28 Five day averaged diffusion of the lighter sediment 44
29 Five day averaged diffusion of the heavier sediment. 45
30 The scaling factor C_1 versus near-bottom concentration 46
31 Time series of median near-bottom sediment concentration 47
32 Typical sediment concentration patches 49
33 The probability of exceeding a certain concentration. 50
34 Probability that the time until the next u_*^c event will exceed X days. 51
35 Log-polar drift plot with alternative h_{max} profile 56
36 Five day averaged diffusion with alternative h_{max} profile 57

List of Tables

1 Friction velocity alternatives 10
2 Differences between u_* derived from 3 and 1 mab currents 10
3 Summary of friction velocity climatology 17
4 Parameter value summary for Hibernia `1b1t` runs 19
5 Monthly median height statistics for u_{*cw} (h_{max} = 9.6m 27
6 The sensitivity of the mean drift to shear above 10 m 32
7 The sensitivity of the diffusivity to shear above 10 m 32
8 Drift climatology for the lighter sediment 39
9 Drift climatology of the heavier sediment 40
10 Diffusivity climatology of the lighter sediment 41
11 Diffusivity climatology of the heavier sediment 42
12 Summary of typical drift and diffusion 48
13 Diffusivity quartiles for the three settling velocities 48

Abstract

Tedford, T., A. Drozdowski and C.G. Hannah, 2003. Suspended Sediment Drift and Dispersion at Hibernia. Can. Tech. Rep. Hydrogr. Ocean Sci. 227: vi+47 p.

The benthic boundary layer transport model (BBLT) was used to characterize the likely drift and dispersion pathways of drill muds discharged from the Hibernia platform on the Grand Banks. The analysis consisted of a series of 3 day model runs covering more than 2 years of current meter observations. The drift was generally to the northwest or the southwest although drift in all directions was observed. The diffusivity was highly variable with monthly diffusivity statistics showing standard deviations larger than the mean. A novel stress dependent settling velocity was used to assess how flocculation and breakup would affect the magnitude and frequency of high concentrations of drill mud near the sea floor. The new formulation did not affect the magnitude or frequency of the high concentration events because only 30% of the simulations experienced breakup. The effect of floc breakup was to reduce the near-bottom concentrations in simulations with low and intermediate concentrations.

Résumé

Tedford, T., A. Drozdowski and C.G. Hannah, 2003. Suspended Sediment Drift and Dispersion at Hibernia. Can. Tech. Rep. Hydrogr. Ocean Sci. 227: vi+47 p.

Le modèle de transport dans la couche benthique (BBLT) a été employé pour caractériser le déplacement probable dû à la dérive et à la dispersion des boues de forage déchargées de la plateforme de Hibernia sur les Grands Bancs. L'analyse se composait d'une série de simulations de 3 jours couvrant plus de 2 ans d'observations de courantomètres. La dérive était généralement en nordouest ou en sudouest bien qu'on ait observé la dérive dans toutes les directions. La diffusivité était fortement variable avec des statistiques mensuelles de diffusivité montrant des écarts type plus grands que la moyenne. Une nouvelle vitesse de dépôt dépendante des efforts a été employée pour évaluer comment la floculation et la fragmentation affectent l'importance et la fréquence des concentrations élevées des boues de forage près du fond sous-marin. La nouvelle formulation n'a pas affecté l'importance ou la fréquence des événements de concentration élevée parce que la fragmentation était présente dans seulement 30% des simulations. L'effet de la fragmentation des floculs a été de réduire les concentrations proche du fond dans les simulations avec des concentrations basses et intermédiaires.

1 Introduction

This report describes the application of SEDTRANS (benthic boundary layer transport model; Sherwood et al. 1999; Telford et al. 2001) to predict the drift and dispersion of suspended drill muds near the petroleum drilling platform at Hibernia, on the Grand Banks (Figure 1). The motivation is to provide a characterization of the benthic dispersion as a first step in the process of interpretation of observed drilling waste distributions. The focus of this study is on the sensitivity of the drift and dispersion to variability in the physical environment and the uncertainty in the bottom stress calculation and particle settling velocity. A novel aspect of this study is a stress dependent particle settling velocity that captures the main features of the flocculation of drill mud from in the marine environment.

The period considered is the one year interval from March 1999 through May 2000 when there was current meters at 3 m and 11 m above the bottom near the Hibernia site (Cranford et al. 2001). Surface wave observations for the same period are combined with the near-bottom currents to derive bottom stress estimates that include the effects of both waves and currents using the computer program SEDTRANS96 (Li and Amos, 2001).

In order to characterize the drift and dispersion we considered a series of 3 day SEDTRANS simulations covering the entire period of the current meter deployment. The ensemble of runs provides information on the drift, dispersion, and concentration characteristics. Each run started with an initial release of 20 metric tonnes of material assumed to reach the seafloor. While there is very little quantitative information available on drill mud discharges at Hibernia, this is not a major concern for this study as it is not concerned with absolute concentration levels. This study is focused on the characterization of the drift and dispersion and understanding how concentration levels can be expected to change due to differences in waves, currents, and bottom stress.

The report is structured as follows. Section 2 presents summaries of the currents and wave data, settling velocity and the friction velocity calculation. The section also describes the method for estimating the maximum height of suspended sediment based on the available CTD profiles and the other input parameters required to run SEDTRANS. In section 3 the relevant derived quantities and the basic elements of SEDTRANS output are discussed. Section 4 investigates how the height of the suspended sediment concentration profile depends on the settling velocity and the details of the friction velocity calculation. Section 5 discusses the sensitivity of the SEDTRANS simulations to the details of the friction velocity calculation and the method chosen to extrapolate the currents to heights above the upper current meter. Section 6 presents the results of the SEDTRANS runs using the entire 3 years of current meter data. In Section 7 the findings of the work are summarized and discussed.

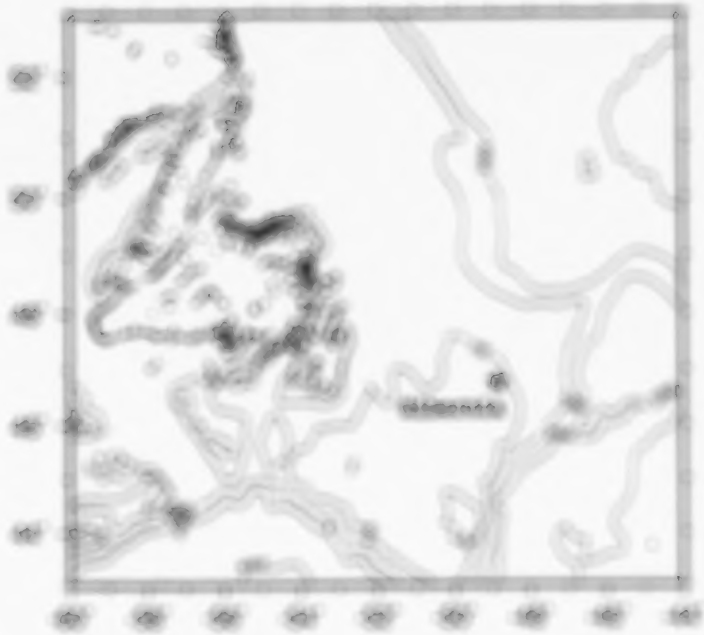

Figure 1: Hibernia location map

2 Model Inputs

This section summarizes the most critical input data and parameters required by wave field data include the currents and wave data and bottom stress (or friction velocity). Required parameters include settling velocity and maximum sediment height. The various methods of calculating friction velocity are outlined and compared. The method for estimating the maximum height of suspended sediment based on the available CTD profiles is described. The primary inputs, outputs and processes in SSTS are shown in Figure 2.

2.1 Currents and Waves

Current data were collected for a one year period at 3 and 10 mab (meters above bottom) within 3 km of the Hibernia platform (Craboltt et al., 2001). The sampling interval was 1 hour. These measurements are assumed to represent the currents in the vicinity of the platform, but they do not represent the way-field which is likely affected by the presence of the platform.

The magnitude of the 3 and 10 mab currents are plotted in Figure 3. The currents show significant variability but no obvious seasonality however they appear to be stronger

Figure 3: Schematic illustrating interaction between data and SENTRANNS. Various items, the boxes, models and various setting on the primary components of the data model.

during March through August from during September to February. Gabbidon et al. (2001) compared the previous the contents of 1 unit. The largest year was observed with the 58 total current, followed by decreasing order by the 51 current, the seventeenth most (3 days), and the second period (9 hours).

Wave observations were obtained from coastal SANNSAB data provided by SMRC Santa and Instrumentation (Br. Abbey, NY), and coordinate the Bureau Program Environment Program. The data were available at the time interval. The data was processed and tested for variations and missing data by Muldrow (2001). The significant wave height and period are plotted in Figure 1. The waves are larger in the fall and with waves.

In Figure 1 a progressive wave diagram is plotted for the current of 1 and 0 unit. The shift is in the northern of 1 unit and is the north of 0 unit. The variance of 0 unit on 995 average (BMR) in average for because the frequency events cannot be combined. In the bay was shift a greater of 1 unit which around was waves and the frequent events.

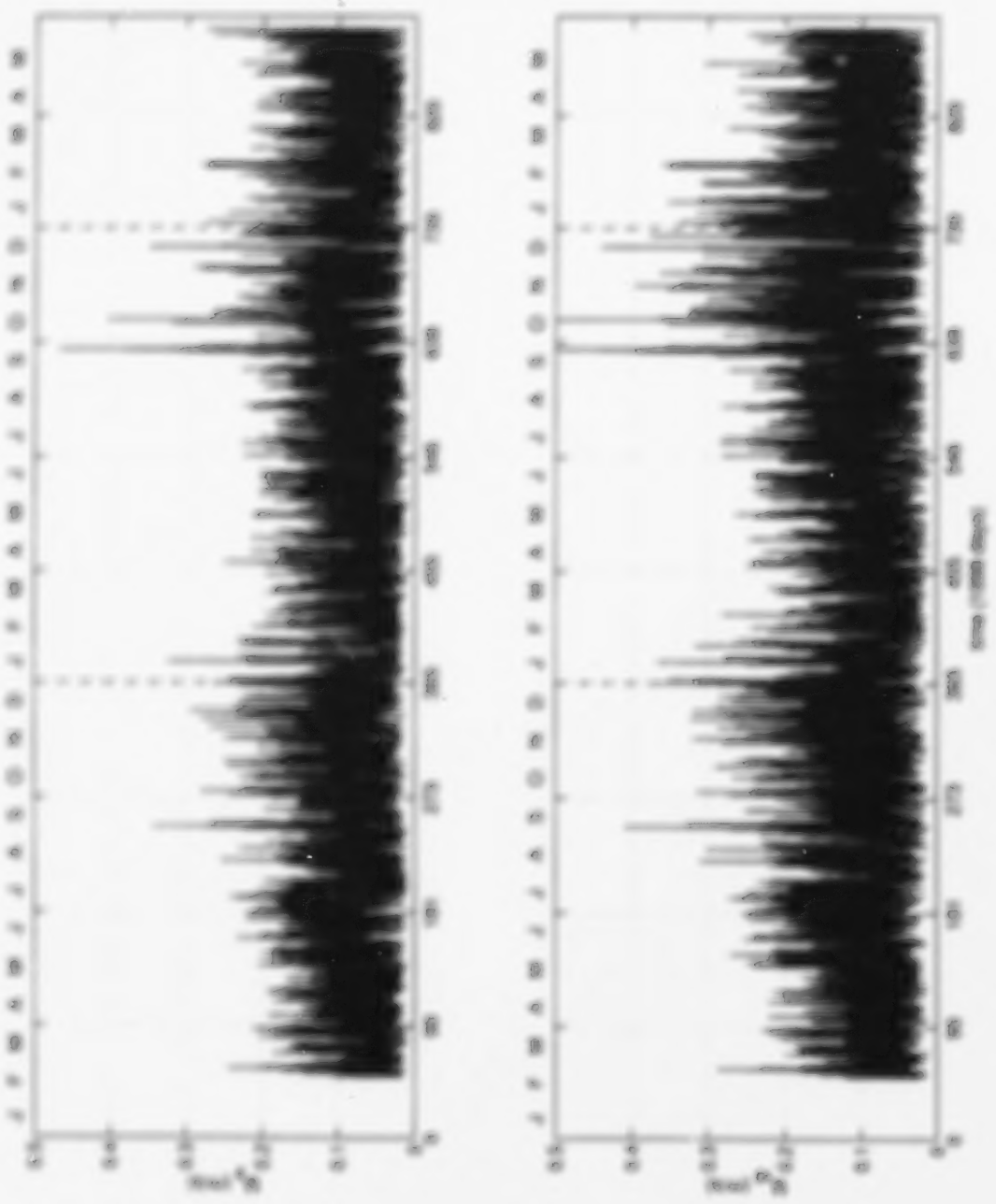

Figure 3: Current magnitude at 3 and 10 meters above horizon.

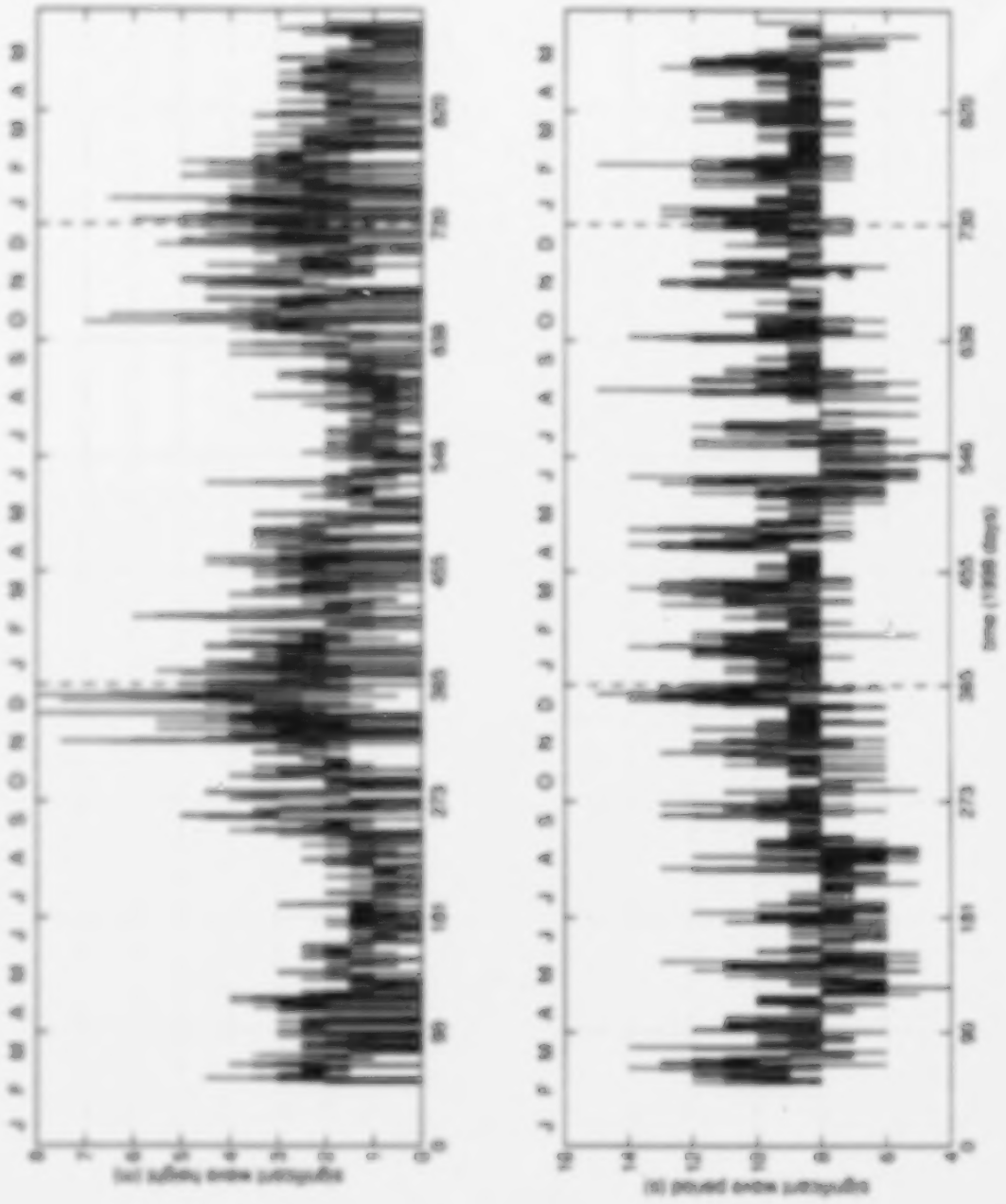

Figure 4: Significant wave bright and period.

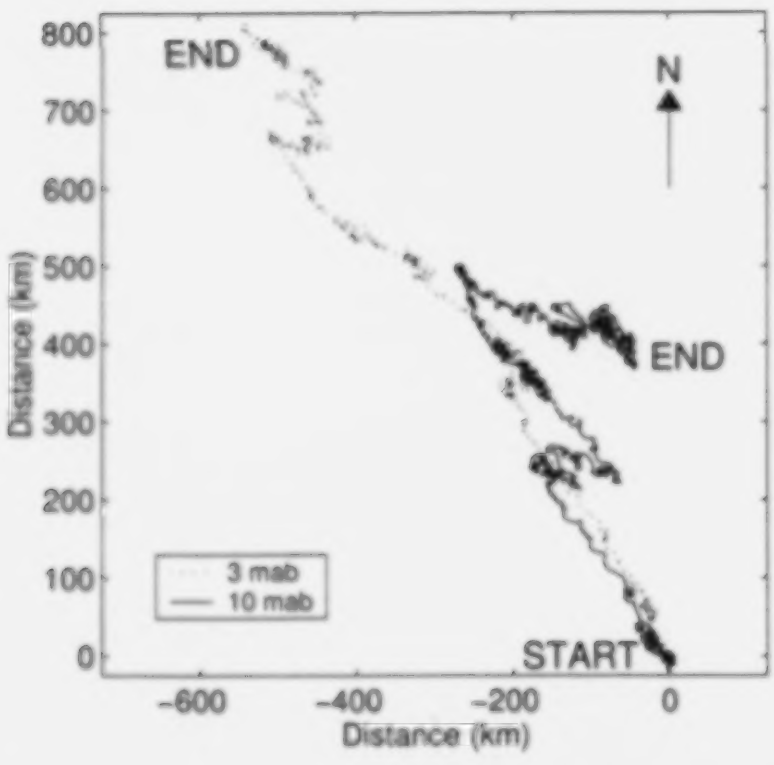

Figure 5: Progressive vector diagram for the two moored current meters.

Velocity Profile Extrapolation

The currents at Hibernia were only available at 3 and 10 mab. It will be shown in section 4 that the median height of the sediment frequently exceeds 10 mab, therefore it was important to estimate the upper currents for modelling purposes. Two alternative methods for extrapolation of currents are considered: 1) set upper currents equal to those at 10 mab; and 2) assume an exponential decay in the velocity gradient with increasing height above bottom. Figure 6 shows two profiles constructed by decreasing the velocity gradient by a factor of e^{-1} every 10 m. This was done for the u and v components independently to generate time series of currents at 7 m intervals above 10 mab. `bblt` used linear interpolation between these 7 m intervals to generate profiles similar to those shown in Figure 6.

2.2 Settling Velocity

In `bblt` the overall (horizontally-averaged) vertical distribution of the sediment is assumed to be governed by an equilibrium concentration profile which is used to derive a

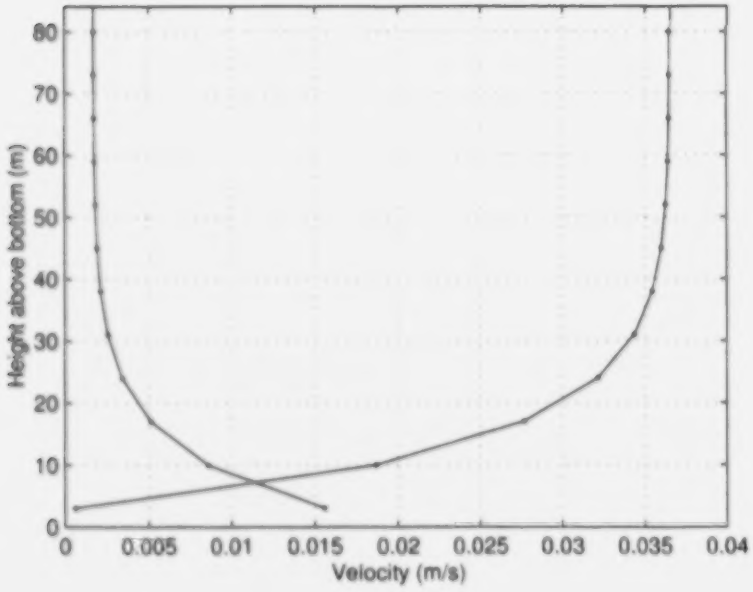

Figure 6: Two sample velocity profile extrapolations constructed with an exponential decay in the observed velocity gradient between 3 and 10 mab.

probability density function for the vertical position of the packets. The concentration profile, $c(z)$, is taken as the Rouse (1937) profile

$$c(z) = c_a(a/z)^p \tag{1}$$

where $z = 0$ at the sea floor and is positive upward, c_a is the concentration at the reference height $z = a$, $p = w/(\kappa u_*)$, w is the settling velocity, the von Karman constant $\kappa = 0.4$, and u_* is the friction velocity. The friction velocity is given by $u_* = (\tau_b/\rho)^{1/2}$, where τ_b is the magnitude of the bottom stress and ρ is the density of water.

Fixed settling velocity

A fixed settling velocity was used for the initial analysis. Two distinct cases were considered: a fast settling velocity $w_0 = 0.5$ cm s^{-1} which will give large near-bottom concentrations under most conditions and a slow settling velocity $w_1 = 0.1$ cm s^{-1} which will give substantially smaller near bottom concentrations. The value for w_0 is the modal value of flocs observed by Milligan and Hill (1998) in their flocculation experiments with water based muds. The value of w_1 is based on settling velocity observations made elsewhere for naturally occurring marine flocs (Hill et al., 1998, 2000).

Stress dependent settling velocity

A simple flocculation routine was incorporated into `bblt` in order to investigate the sensitivity of the results to floc formation and floc breakup. The processes of flocculation and

floc breakup are approximated by making the settling velocity a function of the bottom stress. The flocs are initially assigned the high settling velocity (w_0) to match the large flocs expected to occur in the early stages (high concentration) of the discharge plume. The settling velocity remains at this value until the bottom stress exceeds the critical value u_*^c when the flocs breakup into their individual components and have a very small settling velocity w_2. When the bottom stress becomes less than u_*^c the material flocculates not back to the original size but instead becomes incorporated into the background of marine flocs with settling velocity w_1. Thereafter the settling velocity is w_1 when the stress is less than u_*^c and w_2 when it is greater. The flocculation dynamics are illustrated in Figure 7. We used $w_2 = 0.01$ cm s^{-1}, a small value which leads to nearly uniform vertical distributions under high stress and $u_*^c = 1$ cm s^{-1} (equivalent to 0.1 Pa) for the critical stress of floc breakup (Hill et al., 2001). The settling velocity model proposed here assumes that the flocculation is instantaneous. While not instantaneous, Hill et al. (2001) estimate a flocculation time scale of 900 seconds, which is short compared to the time scales associated with the changes in the bottom stress and the velocity profile. This approach is most applicable to the bulk discharge of water based mud at the end of a drilling section in which case the large discharge gives rise to a high concentration plume where rapid flocculation can occur. The stress dependent settling velocity case will be refereed to hereafter in this report as the variable settling velocity case.

2.3 Friction Velocity

The `bblt` model allows friction velocity, u_*, to be either imported as a time series or calculated from the near-bottom currents. For this project, Anderson (2001) used the sediment transport model SEDTRANS96 (Li and Amos, 2001) to calculate u_* based on the observed currents and waves. The friction velocity is an intermediate output of SEDTRANS96.

SEDTRANS96 requires the following inputs at every time step: water depth, mean current velocity and its direction, height of current measurement above the sea bed, significant wave height, wave period, wave propagation direction, median sediment grain size (diameter) and an initial ripple height and wavelength (Li and Amos, 2001). For this application the grain diameter was set to 0.25 mm based on the surfical sediment type (Anderson, 2001) while the initial ripple height and wavelength were set to values from the previous time step (Anderson Pers. Comm., 1998). The bed-form types and corresponding ripple height and wavelength are calculated by SEDTRANS96.

SEDTRANS96 calculates a friction velocity associated with grain roughness (skin friction) and a friction velocity associated with the flow separation on bed-forms (bed friction). Following the approach of Grant and Madsen (1986), the friction velocity is decomposed into components due to currents only, waves only and the combined effects of waves and currents. We first consider the currents only case (for comparison with the

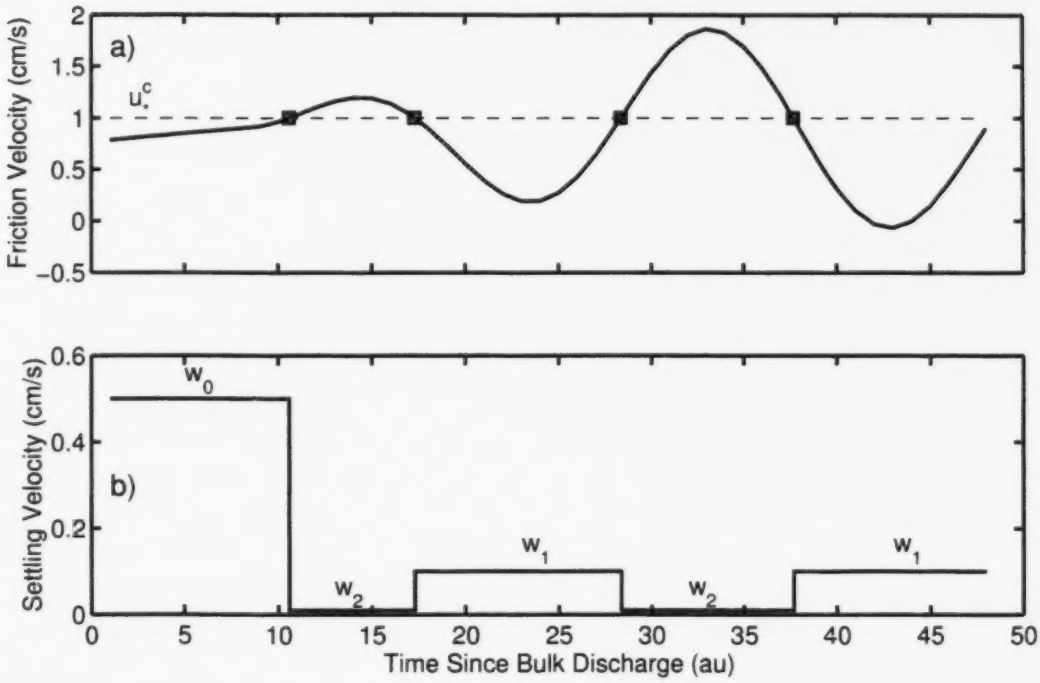

Figure 7: a) Simplified time series of friction velocity. Square markers show when breakup/flocculation occurs. b) Time series of the resulting settling velocity.

default quadratic stress law in `bblt`) and then the combined currents and waves case. The symbols are listed in Table 2.3.

3 and 1 mab currents

The SEDTRANS96 software converts the currents from 3 mab to 1 mab before calculating the stress. The conversion is an iterative procedure which tries to match stress and bed-forms. To help understand the sensitivity of the stress calculation to the iterative procedure, the 3 mab currents were converted to 1 mab current using the fixed ratio of $U_{1m}/U_{3m} = 0.8374$. The scale factor comes from assuming a drag coefficient $C_D = 0.005$ referenced to 1 m. Thus a total of eight u_* time series were considered, four where SEDTRANS96 computed U_{1m} and four where U_{1m} was calculated using the fixed ratio.

The percent difference statistics between u_* based on 3 and 1 mab currents are listed in Table 2. The differences are less than 15.2% 99.9% of the time for all four of the u_* pairs. These discrepancies are small compared to other uncertainties and will be ignored. The set of u_* associated with SEDTRANS96 converting currents from 3 to 1 mab will be the only ones considered in the remainder of this report.

Table 1: Alternative SEDTRANS96 u_* time series

forcing	type of friction	symbol
currents	total(skin plus bed)	u_{*c}
	skin only	u_{*cs}
currents and waves	total(skin plus bed)	u_{*cw}
	skin only	u_{*cws}

Table 2: Statistics of difference between u_* derived from 3 and 1 mab currents. Define $\Upsilon = (u_{*1} - u_{*3})/u_{*3}$.

	$\overline{\Upsilon}$	$\overline{\lvert\Upsilon\rvert}$	RMS(Υ)	MAX($\lvert\Upsilon\rvert$)	99.9%ile
u_{*c}	4.6%	5.0%	5.5%	42.0%	15.2%
u_{*cs}	5.6%	5.7%	6.1%	8.3%	8.1%
u_{*cw}	3.6%	3.6%	4.4%	57.8%	8.0%
u_{*cws}	4.4%	4.4%	5.3%	8.3%	8.0%

Skin vs Total Friction

The skin friction controls the rate of resuspension while the total friction controls the vertical distribution of suspended sediment. However in its present configuration `bblt` does not distinguish between them. The uncertainties in the bed-form calculations necessitate the consideration of both the skin and total (skin+bed) friction velocities. The difference between the friction velocity based on total friction and skin friction is plotted in Figure 8. There are three groups of differences; approximately 2% are 20 to 70% different with the skin friction being less than the total; 80% are identical, and 18% are 5% different with the skin friction greater than the total. The reasons why SEDTRANS96 produces total friction less than skin friction about 20% of the time is not clear, however the differences are consistently small at 5% and will be ignored. Because the average difference is so small (<0.5%) the climatological means presented later are practically the same for the skin and total friction. The sensitivity of `bblt` results to skin vs total friction will be evaluated in Section 5.

Default `bblt` Friction Velocity

In its default mode `bblt` computes a friction velocity (u_{*d}) using a quadratic drag law and a fixed drag coefficient $C_D = 0.0035$ at 3 mab and $C_D = 0.005$ at 1 mab. Note that in the absence of waves SEDTRANS96 uses a drag coefficient of $C_D = 0.003$ at 1 mab. Later on this Section and in Section 5, u_{*d} is compared to the other friction velocities. Outside of this however, u_{*d} was not used for any calculations.

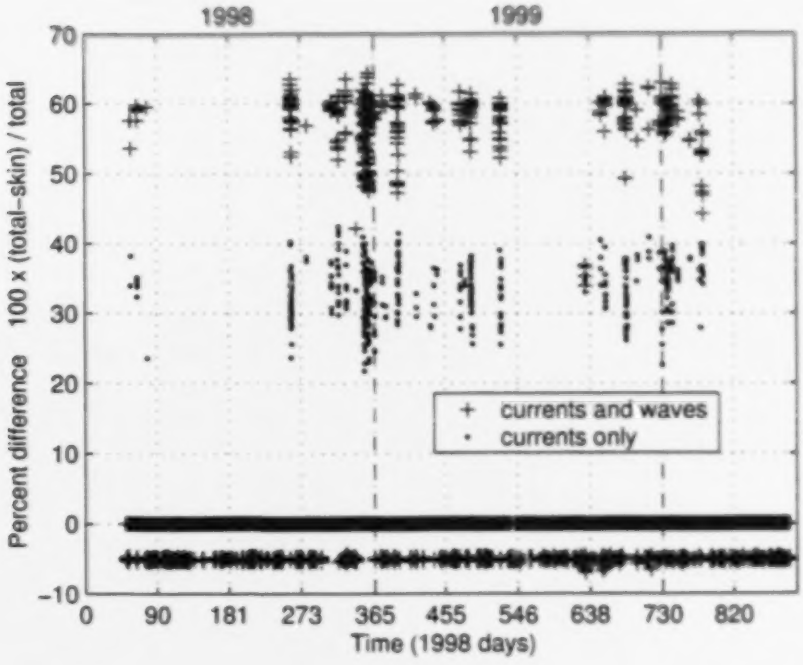

Figure 8: Difference between total friction velocity and skin friction velocity.

Statistics and Climatology

The time series and monthly statistics for u_{*c} u_{*cw} and u_{*d} are plotted in Figures 9 and 10. u_{*d} is usually (>95% of the time) larger than u_{*c}. The SEDTRANS96 u_{*c} is on average 30% less than u_{*d}. Both u_{*d} and u_{*c} show little variation from month to month and very little seasonal variation. The currents and waves friction velocity (u_{*cw}) shows some seasonality with higher values occurring in late fall and early winter. The seasonality of both u_{*c} and u_{*cw} is more apparent in the standard deviation and the maximum than in the mean. There is also considerable variation between 1998 and 1999, especially in December. The climatology is plotted in Figure 11 for u_{*c} and u_{*cw} and summarized in Table 3.

2.4 Maximum Sediment Profile Height

The Rouse profile which defines the vertical distribution of sediment in `bblt` was derived for an unstratified fluid (Rouse 1937). The waters near Hibernia however exhibit significant stratification during much of the year. Figure 12 shows density profiles from 12 CTD casts done during the summer and fall of 1998, 1999 and 2000. The profiles show a surface mixed layer and/or a bottom mixed layer.

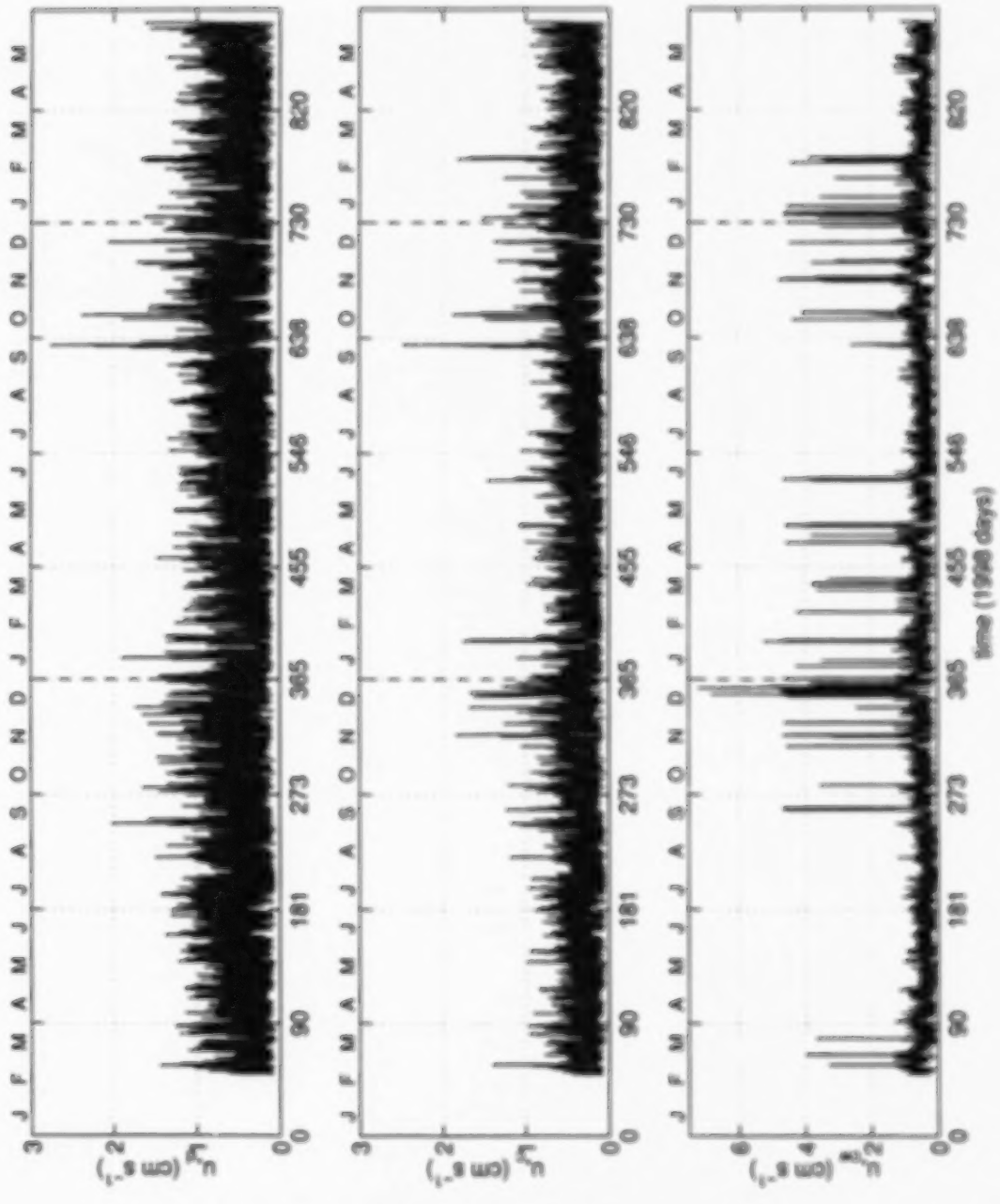

Figure 9: Hourly friction velocity for u_{*d}, u_{*c} and u_{*cw}.

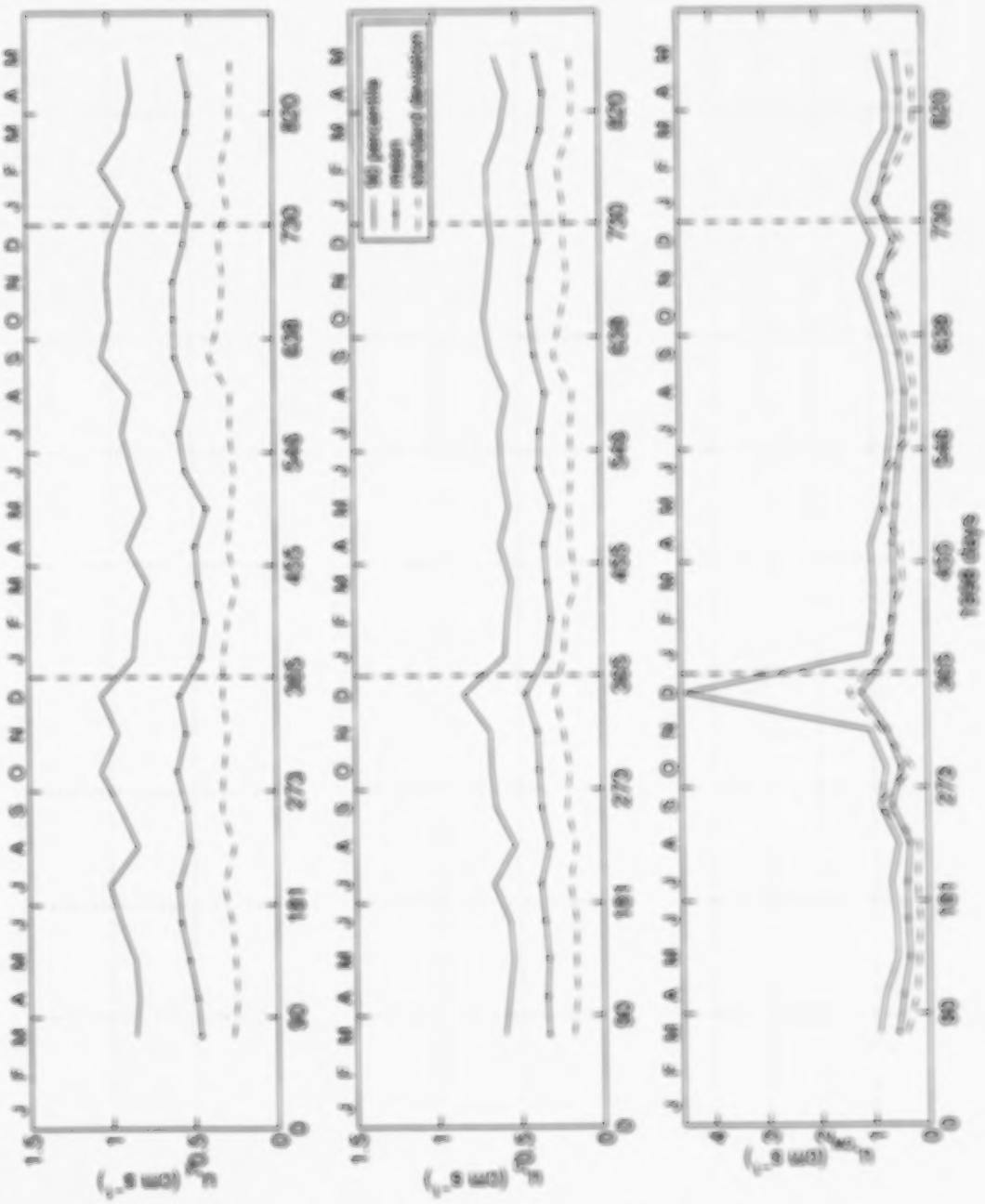

Figure 10: Monthly friction velocity statistics for $u_{*\theta}$, u_{*w} and u_{*uw}.

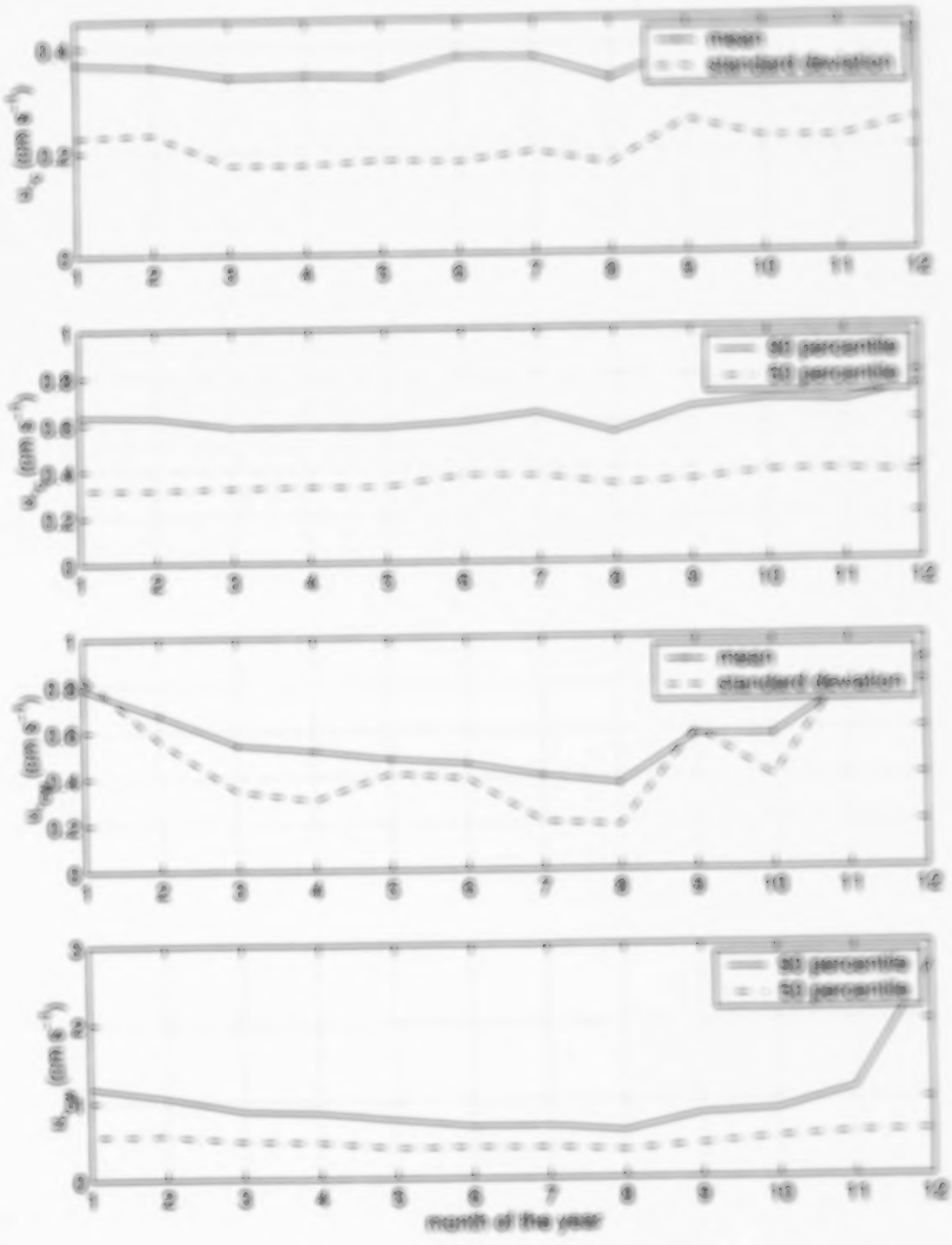

Figure 11: Seasonal climatology for v_{sfc}, v_{bc}, and v_{cm}.

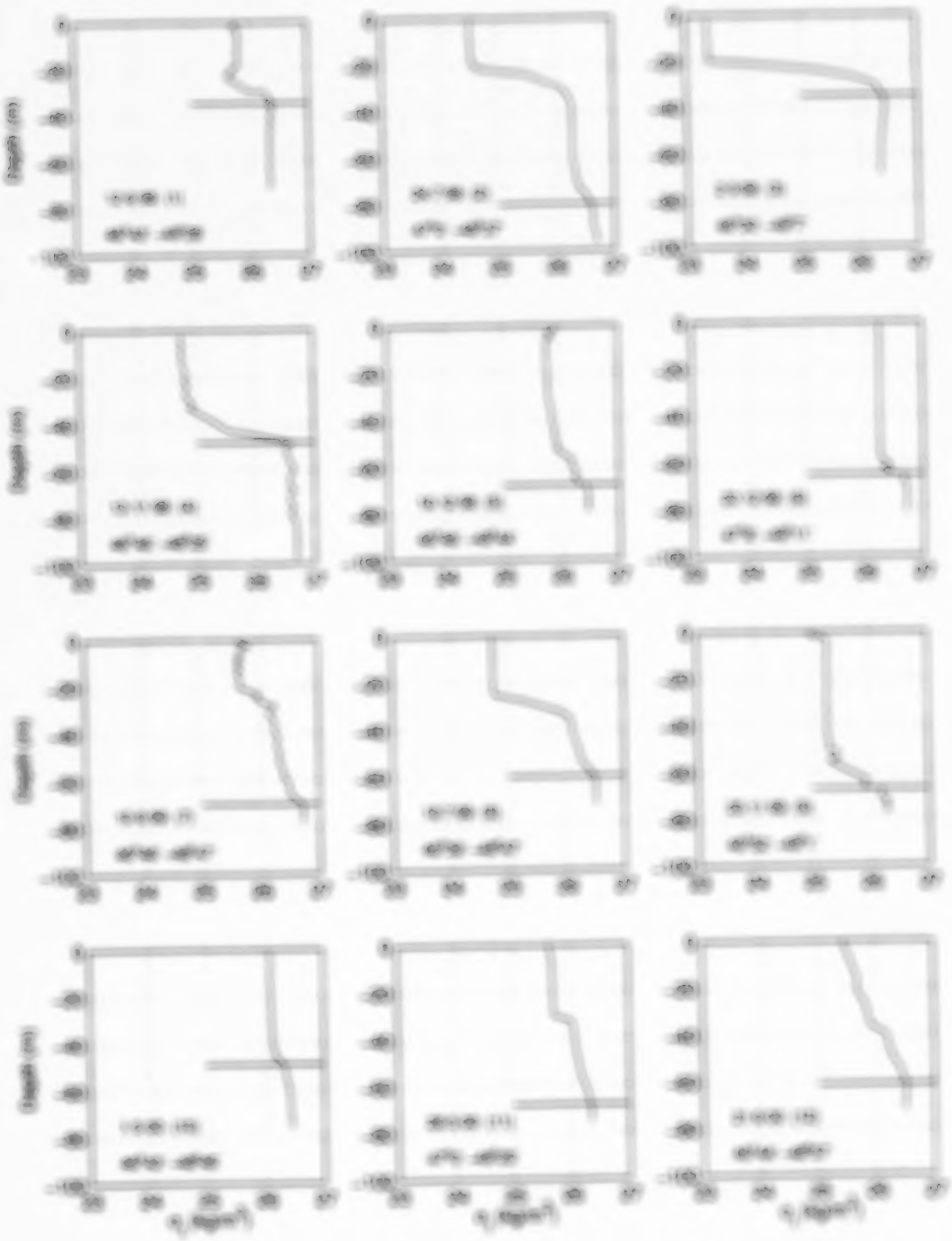

Figure 12: Density profiles observed at Ellesmin during the period of interest. The horizontal line shows depth chosen for h_{max}.

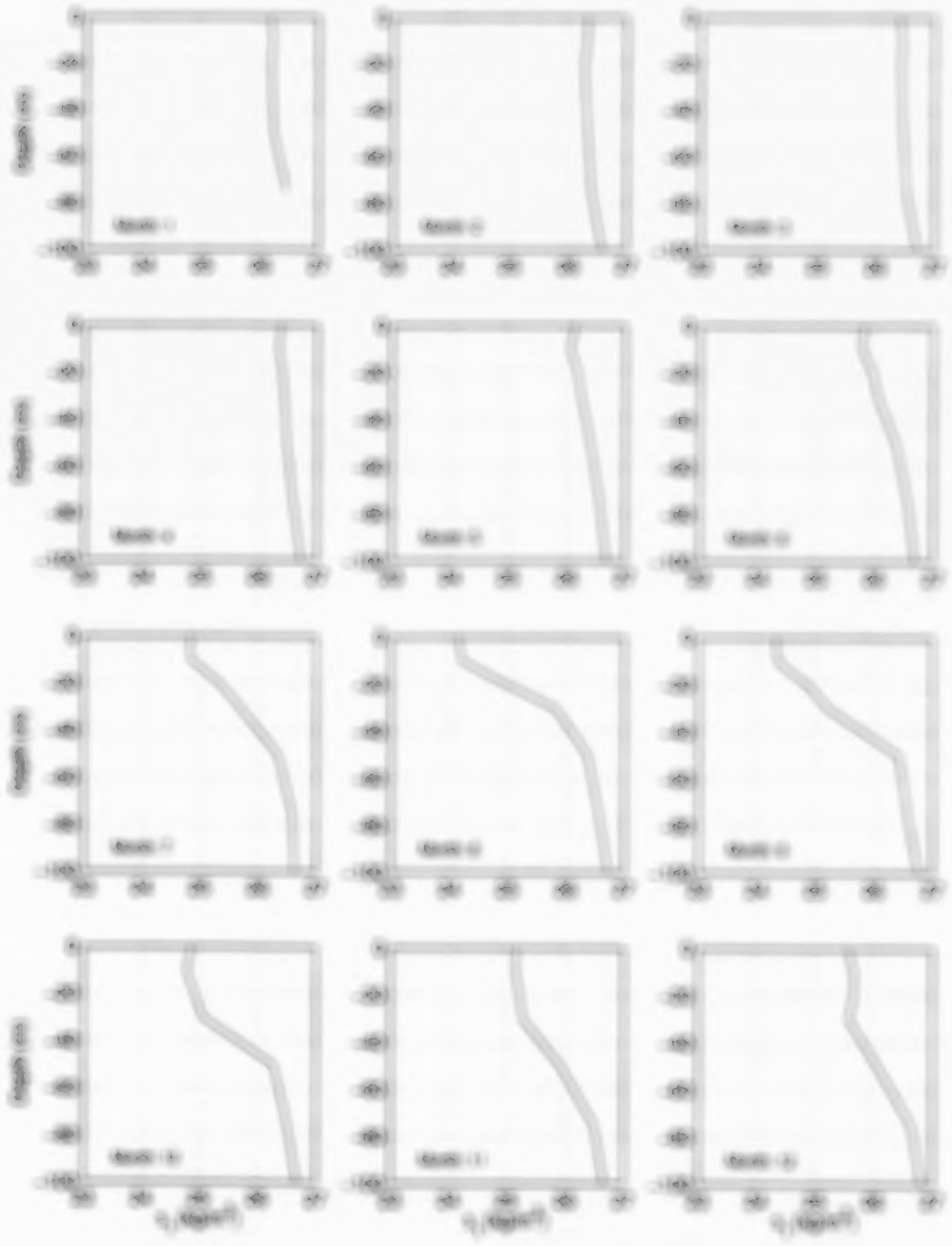

Figure 10: Seasonal density profiles in the vicinity of Ellsworth (Pierce, 2002 pers. comm.)

Table 6: Summary of filtration velocity climatology for the optical-depth record. The N column corresponds to the number of available data points for each month.

		v_{fil}			$v_{\mathrm{fil,\,clim}}$		
Month	N	mean	stddev	Max	mean	stddev	Max
Jan	1648	0.37	0.28	1.83	0.70	0.66	2.81
Feb	1449	0.39	0.31	1.89	0.67	0.64	3.15
Mar	2032	0.33	0.17	0.97	0.53	0.33	2.08
Apr	2169	0.33	0.17	0.99	0.53	0.40	3.29
May	2002	0.33	0.18	1.09	0.49	0.45	3.33
Jun	1993	0.36	0.18	1.14	0.49	0.39	3.29
Jul	1649	0.40	0.29	1.83	0.49	0.53	3.68
Aug	1455	0.39	0.27	1.89	0.57	0.58	3.27
Sep	1649	0.40	0.31	1.89	0.57	0.60	3.65
Oct	1455	0.41	0.31	1.91	0.57	0.58	3.59
Nov	1649	0.41	0.32	1.89	0.70	0.65	3.75
Dec	1455	0.41	0.30	1.91	0.69	0.64	3.65

Starting at the bottom and moving up, the first sharp density gradient encountered (a gravicline) was assumed to represent the top of the frozen gravity layer. Sublayer segments above this height (h_{max}) was assumed to be negligible. Figure 4 shows horizontal lines for the heights at which the gravicline was found. If the gravicline was not found (as in February, March and April for most years), it was considered to exist above the highest density gradient observed for the year. The maximum sublayer gravity height for those months was taken to be equal to the height of the water-wave column. The time series of h_{max} for the entire record was reconstructed from the 2-D profiles (Figure 11). One notable exception was the location of 1 m below the bottom of the density profile. The other exception was the location 0.25 m (the sounding depth at the current meter location). The most striking difference between the two occurs in July 1999 when the density profile goes to 0.9 m depth and $h_{\mathrm{max}} = 1$ m is achieved in the version referenced to 0 m. In contrast the version referenced to the bottom of the profile never reaches its minimum possible value of 1 m. This small value ($h_{\mathrm{max}} = 1$ m likely due to the mismatch between the depth where the profile was taken and the depth at the current meter location. The version with h_{max} referenced to the bottom of the density profile is used in the applications reported here. Some results with the second version are reported in Appendix 1 for comparison.

This approach captures the features of the annual cycle of h_{max} but it cannot capture resuspension and deresuspension events in the winter and near the bottom that occur on short time scales.

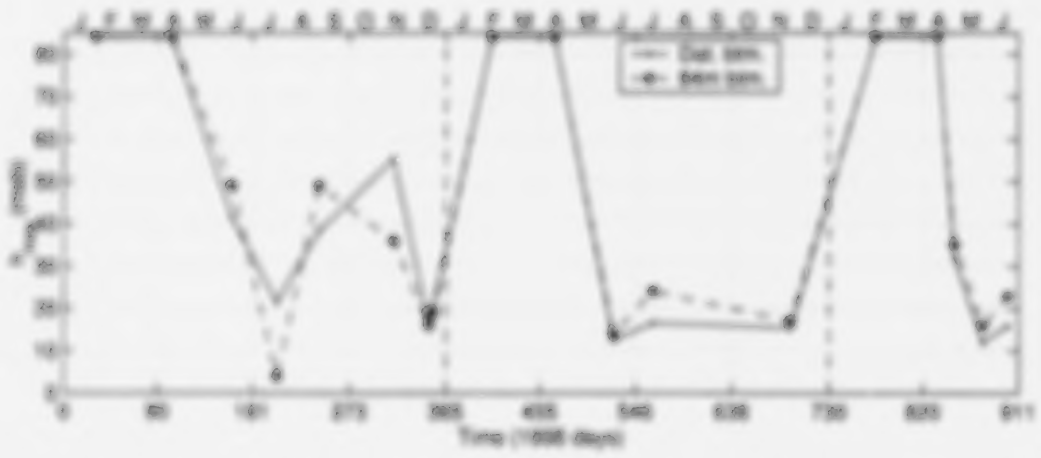

Figure 16: Time series of k_{max} based on available CTD data and the assumption of no stratification in February, March and April.

3.9 Drill Mud Input

Every MAY simulation in this report starts with a bulk release of 20 metric tonnes of material. All of the material is assumed to reach the seafloor. This amount is typical of the amount of barite discharged as part of the water-based-mud (WBM) during the drilling of the initial 'open-circuit' section of a hole on the Scotian Shelf. Thus the near-bottom concentrations can be interpreted as concentrations of barite.

The discharges (and the resulting concentrations) are probably not representative of the amounts of drill mud discharged during the period of the current meter deployment. However there is very little quantitative information available on drill mud discharges at Hibernia to use in estimating mud inputs. We note that the discharges were likely cuttings based muds (SBM) covering the ocean stuck to the cuttings rather than bulk dumps of WBM or direct discharges to the sea floor. Direct discharges to the seafloor are characteristic of the initial phases of drilling before the riser is installed and the drilling circuit is completed. Bulk dumps of WBM occur when WBM is used to drill the deeper portions of the hole, and generally mud formulations other than WBM are preferred by the drillers.

Comparison of the concentrations reported in this report with concentrations observed in the field will have to account for the expected magnitude of the discharges at Hibernia and for the expected fraction reaching the benthic boundary layer. This report does not deal with the convective descent issue of what fraction of the actual discharges reach the sea floor.

Table 4: Parameter values for Hibernia bblt runs.

Parameter	Value
Number of Packets (N)	10^5
Vertical Shuffling Time (t_m)	3.0 hours
Advection Time Step (Δt_a)	0.1 hours
Simulation Period	120 hours
Current meter time interval	1.0 hour
Sediment Mass	20×10^3 kg
Reference Height (h_{ref})	0.0035 m

2.6 Other Input Parameters

The bblt model requires several other inputs that were assigned a single value for this study. The parameters and their value are listed in Table 4.

Number of Packets: In bblt the sediment is partitioned into discrete pseudo particles or packets. The greater the number of packets the finer the spatial resolution of the model results. In this case 10^5 gives adequate resolution and reasonable run time.

Vertical Shuffling Time: In environments where the M2 tidal cycle dominates the current spectrum, as is the case at Hibernia, this parameter is set to 3 hours to maximize dispersion (Hannah et al., 1995). This parameter affects the dispersion but not the mean drift.

Advection Time Step: This parameter controls run time and must be less than half the shuffling time (Hannah et al., 1995). It is set to 0.1 hours in this case to balance the granularity of packet mixing and run time.

Simulation Period: The simulation period was set to 5 days so that during a single run several M2 tidal cycles would occur and the suspended sediment would remain within the current regime described by the collected data.

Current Meter Time Interval: This is specified to match the available current meter data, 1 hour.

Reference Height: The reference height is the lower boundary of suspended sediment. This is set to 0.0035 m to correspond with a roughness length which matches the drag coefficient, $C_D = 0.0035$, used in the construction of the log layer for currents measured at 3 mab.

3 Model Output

The fundamental output from `bblt` is the time series of the positions of the sediment packets. This section describes the post-processing required to obtain more general quantities such as drift rate, diffusivity and near-bottom concentration.

3.1 Derived Quantities

The model outputs are the time series of positions of the packets

$$X_n(t),\ Y_n(t),\ Z_n(t) \quad \text{for} \quad n = 1, \ldots, N \tag{2}$$

where $X_n(t)$ is the x-coordinate of packet n at time t, Y_n is its y-coordinate and Z_n is its vertical coordinate (positive upward from the sea floor). N is the number of packets.

First, we introduce the center of mass of the cloud of packets $(\overline{X}(t), \overline{Y}(t), \overline{Z}(t))$ where

$$\overline{X}(t) = (1/N) \sum_{n=1}^{N} X_n(t) \tag{3}$$

and the other two components are defined in the same manner. We refer to the vertical center of mass $\overline{Z}$ as the 'mean height' of the sediment. The time average of the instantaneous mean height is denoted $< \overline{Z} >$. The mean drift $(\overline{U}, \overline{V})$ is the time rate of change of the horizontal center of mass over the simulation. $\overline{U}$ and $\overline{V}$ are computed as the slope of a straight line fitted to the time series $\overline{X}(t)$ and $\overline{Y}(t)$.

The horizontal spreading of the cloud about its center of mass is measured by the horizontal variance of the packet distribution σ^2. In one dimension the variance of N packets is

$$\sigma^2(t) = \frac{1}{N-1} \sum_{n=1}^{N} (X_n - \overline{X})^2 \tag{4}$$

In two dimensions we calculate σ^2_{max} and σ^2_{min} which are the variances along the major and minor axes of the horizontal projection of the distribution. These axes are computed at regular intervals from the eigenvectors of the horizontal variance matrix.

The effective horizontal diffusivities along the major (K_{max}) and minor (K_{min}) axes are then defined as

$$K_{max} = \frac{1}{2} \frac{\partial \overline{\sigma^2}_{max}}{\partial t} \qquad K_{min} = \frac{1}{2} \frac{\partial \overline{\sigma^2}_{min}}{\partial t} \tag{5}$$

(e.g. Csanady 1973), where the over-bar denotes a time averaging which smooths out short-term fluctuations such as the tides. For a bulk release, analytical solutions to the 2-d diffusion equation (i.e. no advection) indicate that the concentration C, at the source should scale as

$$C \propto 1/\sqrt{K_{max} K_{min}}, \tag{6}$$

(see Fischer et al. 1979; their eq.(2.53)). With advection, the concentration following the (horizontal) center of mass can be expected to follow the same scaling. Therefore for bulk release simulations we generally report $D = \sqrt{K_{max} K_{min}}$ as a measure of the overall rate of spreading (i.e. of the vertically-integrated sediment distribution).

The calculation of concentration (mass per unit volume) uses the number of packets in the specified cylindrical sampling volumes together with the packet mass M. We focus on the near-bottom concentration averaged over the lowest 0.1 m of the profile; i.e. over the vertical interval between $z = h_{ref}$ and $z = h_{ref} + \Delta z_j$ where $\Delta z_j = 0.1$ m.

3.2 Median Height

The median height of the sediment profile can be derived as follows. Let $F(z)$ be the fraction of the material between the bottom (h_{ref}) and the height z. The height for which $F(z) = \alpha$ is (Hannah et al. 1995)

$$z/h_{ref} = \begin{cases} [1 + \alpha[(h_{max}/h_{ref})^{1-p} - 1]]^{1/(1-p)} & p \neq 1 \\ (h_{max}/h_{ref})^{\alpha} & p = 1 \end{cases} \tag{7}$$

where $p = \omega_s/\kappa u_*$. For known p, h_{max}, and h_{ref}, the median height is computed by setting $\alpha = 0.5$.

3.3 Scaling Parameters and Near-Bottom Concentrations

For a bulk release the near bottom concentration following the centre of mass depends on both the diffusivity and the character of the vertical profile of concentration. The 2-d concentration scaling (6) can be extended to the near-bottom concentration by accounting for differences in the vertical extent of the concentration profile. Let $F(z_1)$ be the fraction of mass between the bottom and near bottom height z_1. Then (6) can be modified to be

$$C_1 = F(z_1)/D \tag{8}$$

Since F is a function of the Rouse number p which varies with time as the bottom stress fluctuates. The time average of the sediment's vertical center of mass ($< \overline{Z} >$) is used to calculate an effective Rouse number which is then used to calculate $F(z_1)$. This scaling factor can be compared with the computed concentrations from bulk discharge simulations to help interpret the model results.

4 Median Sediment Height

In this section we show how the bottom stress, settling velocity and h_{max} all play important roles in determining the vertical distribution of the sediment. We consider

the two fixed settling velocities ($w_s = 0.1, 0.5$ cm s^{-1}), three stratification conditions ($h_{max} = 20, 84$ m and h_{max} variable) and two friction velocities. The measure used to describe the vertical distribution is the median height.

The median height is plotted for both settling velocities in Figures 15-17. In Figure 15, h_{max} is equal to the total water depth (84 m), implying negligible stratification. The friction velocity used is u_{*cw}. The median height of the lighter particles ($w_s = 0.1$ cm s^{-1}) frequently approaches mid-depth indicating a near uniform distribution of sediment in the water column. The median height of these particles has minimal seasonality. The median height of the heavier particles ($w_s = 0.5$ cm s^{-1}) rarely exceeds 3 m during the two year period. These particles exhibit some seasonality, with higher suspension events occurring during the late fall and early winter when wave activity is high.

Figure 16 shows the median sediment heights with the seasonally varying h_{max}. For $w_s = 0.1$ cm s^{-1}, the varying h_{max} has a strong influence on the sediment suspension. Particles are generally forced to remain lower in the water column during the summer and fall. For $w_s = 0.5$ cm s^{-1}, the sediment remains very close to the bottom and has little dependence on the variations in h_{max}.

Figure 17 shows the median sediment heights with h_{max} fixed at 20 m. The results are qualitatively similar to those for $h_{max} = 84$ m. Accordingly, the h_{max} parameter is approximately a scaling factor in the sediment profile determination. Close comparison of Figures 15 and 17 shows the influence of h_{max} decreases as the median height approaches zero.

The monthly mean and standard deviation of the median heights are plotted in Figure 18 and tabulated in Table 5. The patterns in Figure 18 are similar to those shown in Figure 10 for the monthly u_{*cw} statistics; the average median height is the greatest in the late fall and early winter and the lowest in the summer. The average median height of the heavier sediment approaches zero in the summer (Table 5) indicating very little suspension during this period. The summer may or may not be the period of the greatest impact as this is also a time of strong stratification when releases of drill mud in the upper or mid water column have less potential to reach the bottom.

Figure 19 shows a comparison of the median height with (u_{*cw}) and without (u_{*cws}) the contribution from the bedforms. Most of the differences are small as discussed in Section 2.3. The heavier sediment exhibits greater differences in median height with the additional bed-form stress. This difference in sensitivity is a consequence of the lighter sediment approaching the limit of a uniform vertical distribution with only the skin friction velocity and therefore showing no change with increased stress.

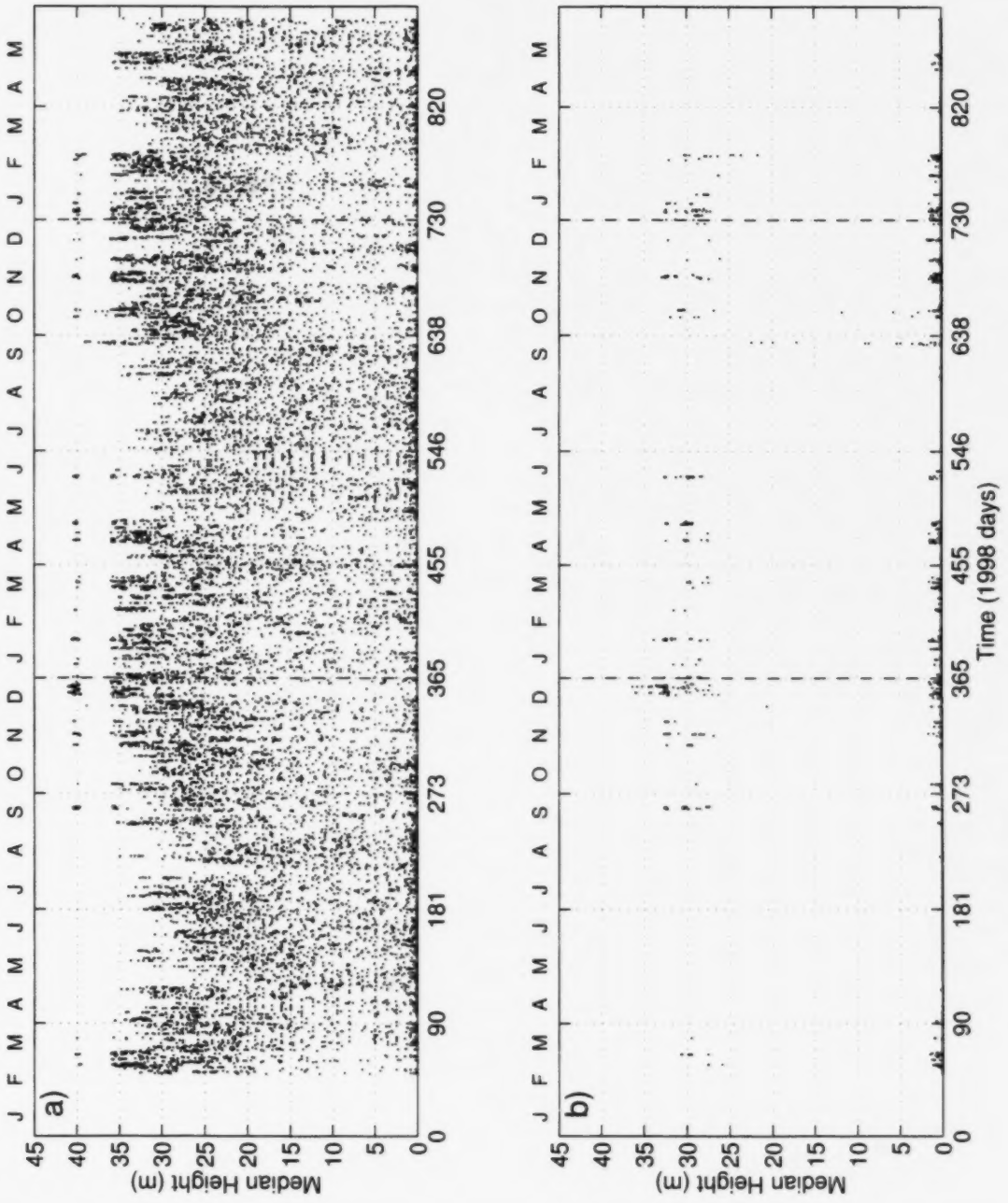
a)
b)
J F M A M J J A S O N D J F M A M J J A S O N D J F M A M
0 90 181 273 365 455 546 638 730 820
45 40 35 30 25 20 15 10 5 0
Median Height (m)
Time (1998 days)

Figure 15: The hourly median height of sediment particles for a) $w_s = 0.1$ cm s^{-1} and b) $w_s = 0.5$ cm s^{-1}. The maximum profile height, h_{max}, is equal to the total depth (84 m).

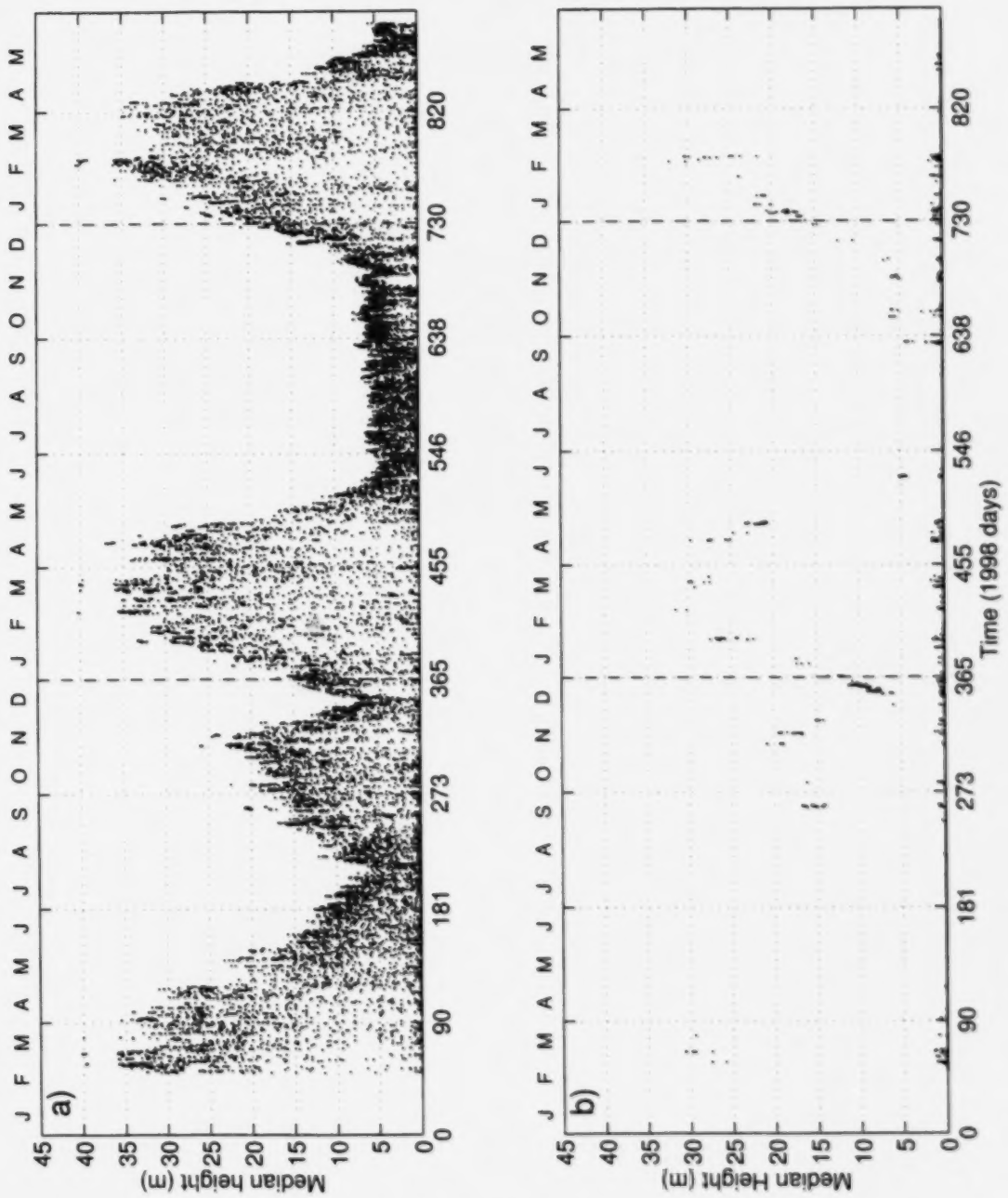
a)
b)
Median height (m)
Median Height (m)
Time (1998 days)
J F M A M J J A S O N D J F M A M
0 90 181 273 365 455 546 638 730 820
0 5 10 15 20 25 30 35 40 45

Figure 16: The median height of sediment particles for a) $w_s = 0.1$ cm s^{-1} and b) $w_s = 0.5$ cm s^{-1}. The maximum profile height, h_{max}, varies.

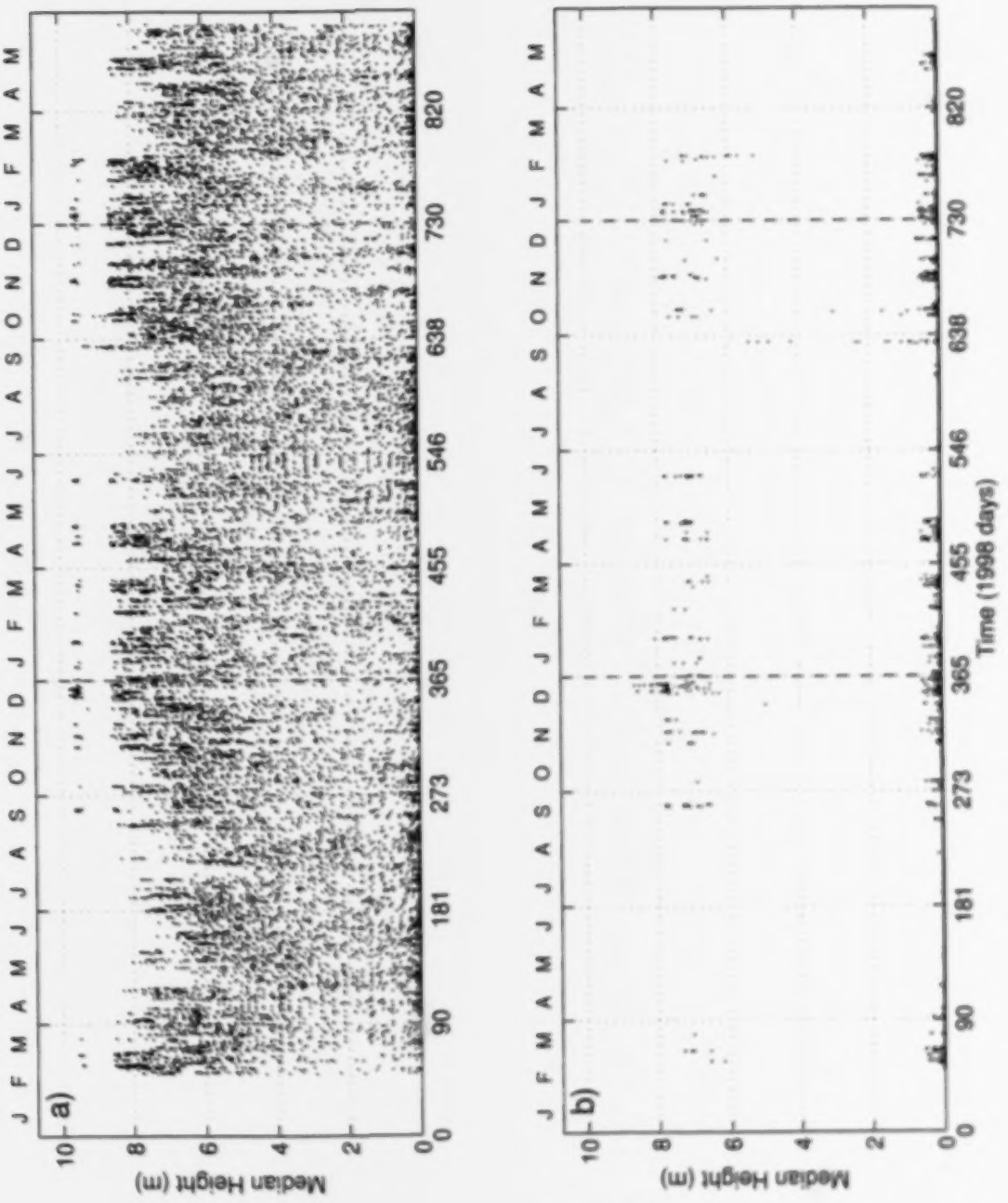

Figure 17: The hourly median height of sediment particles for a) $w_s = 0.1$ cm s^{-1} and b) $w_s = 0.5$ cm s^{-1}. The maximum profile height, h_{max}, is equal to 20 m.

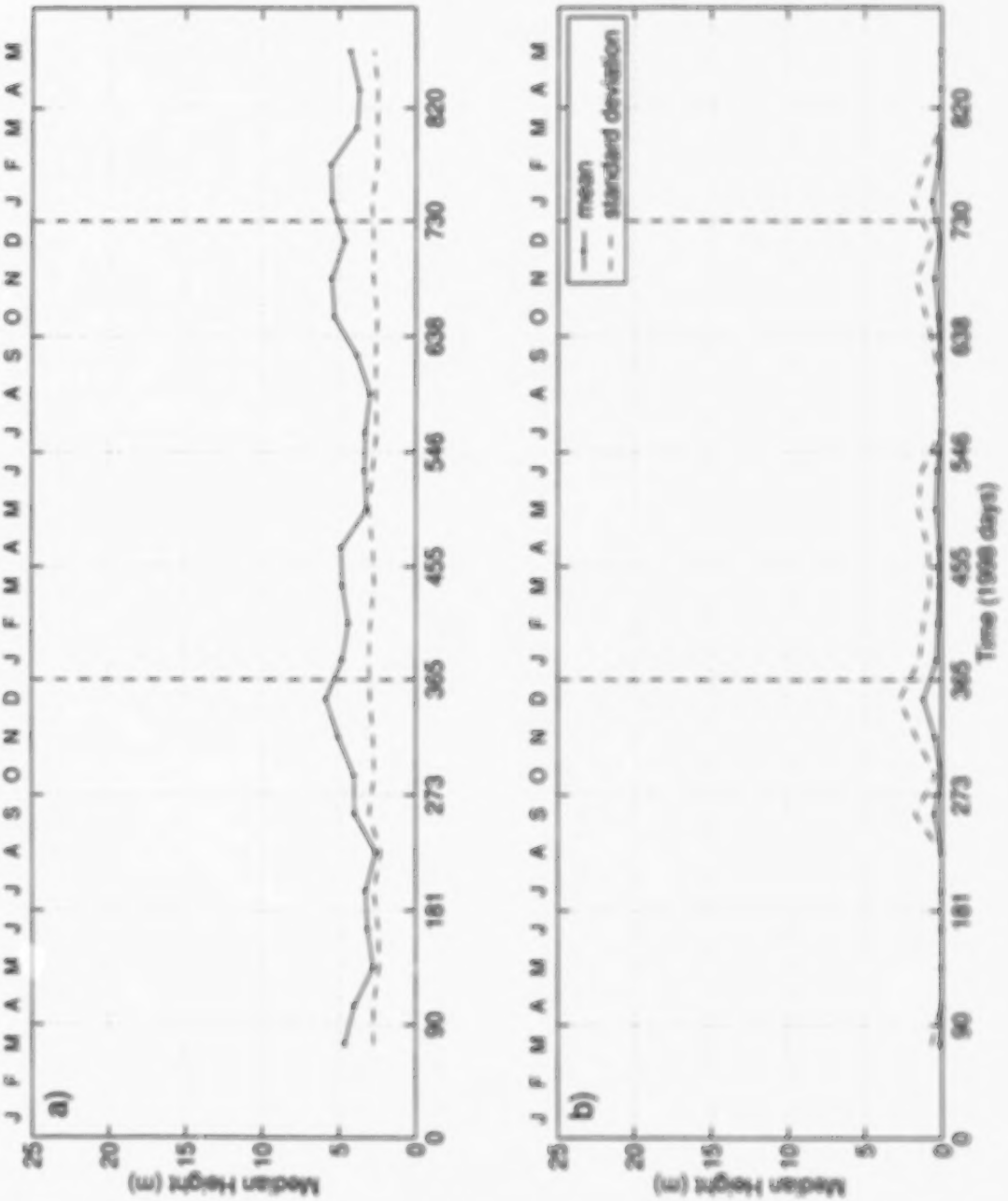

Figure 18: Monthly median height calculated with u_{rms} and $h_{max} = 84$ m. a) $w_s = 0.1$ cm s^{-1}, b) $w_s = 0.5$ cm s^{-1}.

Table 5: Monthly median sediment height (in meters) for w_{wave} ($h_{wave} = 0.6$m).

			$w_s = 0.1$ cm s^{-1}		$w_s = 0.5$ cm s^{-1}	
Month	Year	N	mean	stddev	mean	stddev
Mar	98	744	19.2	11.7	0.3	2.9
Apr	98	720	16.4	11.6	0.01	0.05
May	98	744	11.1	9.9	0.01	0.003
Jun	98	720	12.7	10.2	0.01	0.002
Jul	98	744	13.3	11.4	0.01	0.004
Aug	98	744	10.4	9.5	0.01	0.01
Sep	98	720	16.4	12.9	1.9	7.3
Oct	98	744	16.4	11.4	0.1	1.5
Nov	98	720	20.9	11.8	1.7	6.9
Dec	98	744	24.4	12.6	4.9	11.5
Jan	99	744	19.8	12.8	1.3	6.0
Feb	99	672	18.1	12.4	0.8	4.9
Mar	99	744	19.7	11.4	0.4	3.1
Apr	99	720	20.1	11.8	0.5	3.6
May	99	744	13.0	12.9	1.4	6.3
Jun	99	720	13.5	11.8	1.0	5.4
Jul	99	744	13.3	10.7	0.01	0.003
Aug	99	744	11.9	10.8	0.01	0.01
Sep	99	720	15.6	11.0	0.2	1.6
Oct	99	744	22.0	10.5	0.6	4.1
Nov	99	720	22.8	11.6	1.7	6.9
Dec	99	744	19.0	11.6	0.3	2.8
Jan	00	744	22.7	12.1	2.3	7.9
Feb	00	672	23.0	10.6	0.8	4.4
Mar	00	744	15.6	10.5	0.01	0.01
Apr	00	720	15.0	10.4	0.01	0.01
May	00	744	17.5	11.4	0.02	0.1

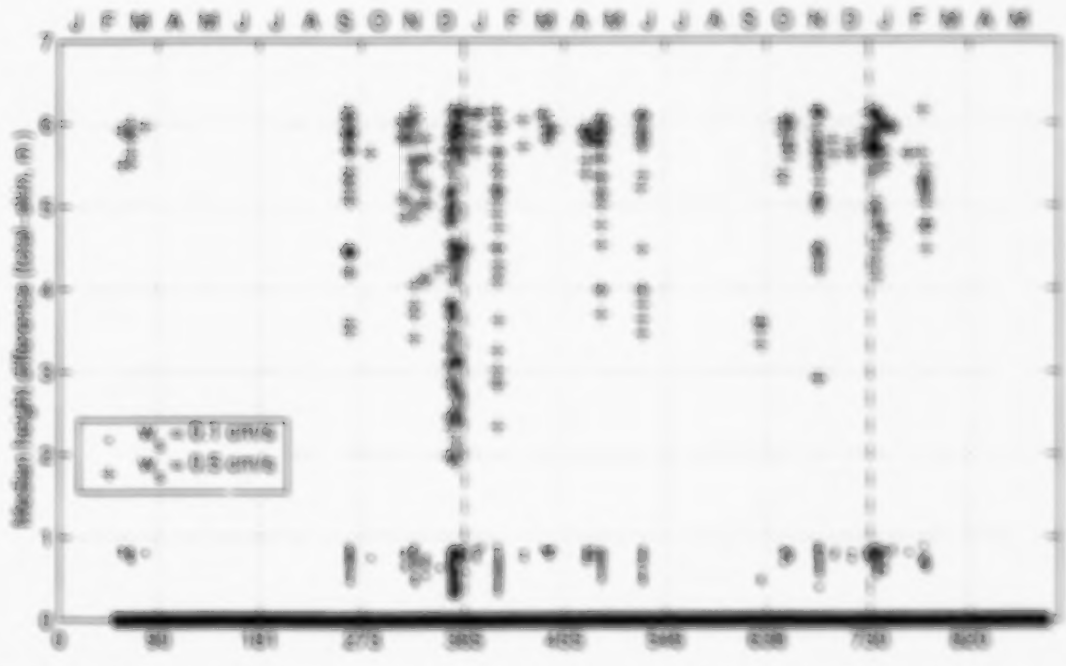

Figure 19: The difference between the hourly median height associated with the total friction velocity (u_{*tot}) and the skin friction velocity (u_{*skin}). The maximum profile height, h_{max}, is equal to 20m.

5 Sensitivity Analysis

This section will discuss the sensitivity of model results to the choice of currents extrapolation and friction velocity. The two alternatives for the velocity extrapolation above 10 m are a zero velocity gradient and an exponential decay in the velocity gradient. Four different friction velocities are considered: u_{*db}, u_{*c}, u_{*tot} and u_{*skin}. This gives eight alternative scenarios for each of the two fixed settling velocities; sixteen alternatives in total. The analysis consisted of carrying out several runs for each scenario and comparing their statistics.

Figure 20a indicates the times when the model runs were performed. For each scenario the model was run consecutively 24 times, with runs beginning every 2.5 days. The runs were five days long and h_{max} was set to 20 m. The first run begins on October 13, 1999 (1999 day 650) and the last run finishes at noon on December 14, 1999 (1999 day 712.5). This interval was chosen as it includes periods of low and high u_{*c} values. There is an apparent 14 day periodicity seen in the 5-day averages. Figure 20b shows the bottom current and tidal analysis for the period. The phase of the spring-neap cycle does not match the peaks and troughs in the currents or the bottom stress. Therefore the tidal

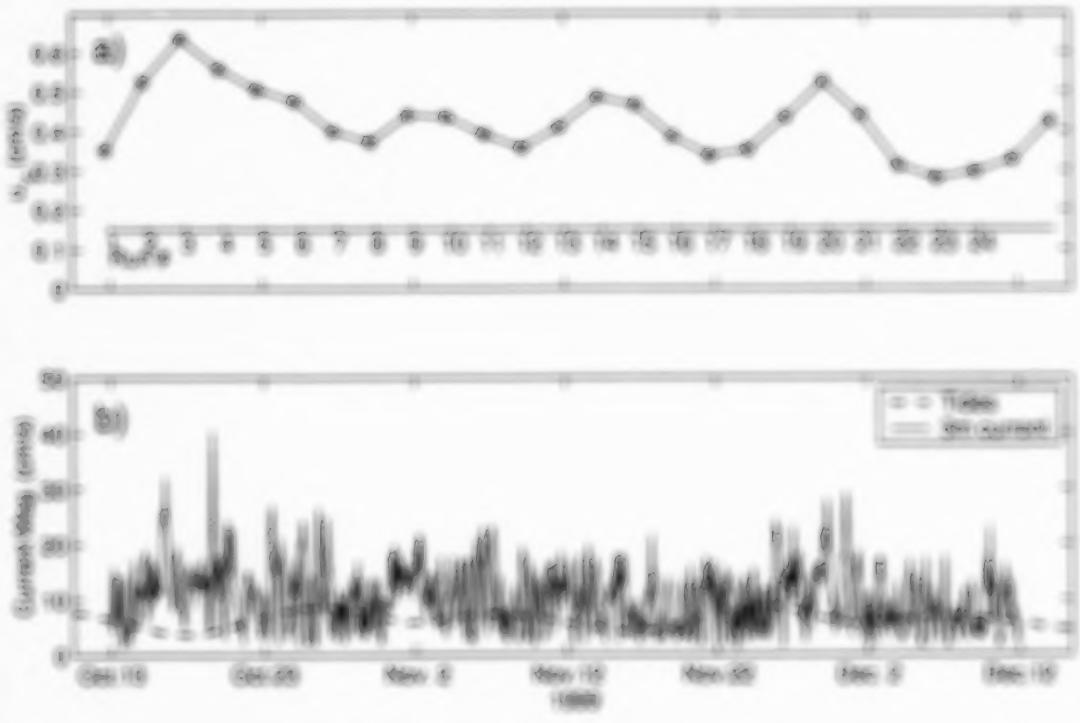

Figure 20: a) Five day averages of ϵ_{tke}. b) Magnitude of the currents. Also shown is the envelope of the tidal current due to M2, N2 and S2 based on tidal analysis for entire record. Notice that the tidal current is small relative to the bottom current and that the peaks of the spring/neap cycle do not match the peaks in the current and bottom stress.

currents are unlikely to be the cause of the apparent periodicity.

Drift

The mean drift for each simulation with $\omega_o = 0.1$ cm s^{-1} is plotted in Figure 21. The drift has a northwest-southeast orientation. The average drift for each bottom stress and shear shape combination is summarized in Table 6. The differences between the drift with and without shear shape and with and without bed-form friction (ϵ_{tke} versus $\epsilon_{tke,nf}$) are both negligible. The ϵ_{ust} drift is on average slightly greater than the ϵ_{tke} and $\epsilon_{tke,nf}$ drift. Similarly, the ϵ_{cd} drift is less than the ϵ_{tke} and $\epsilon_{tke,nf}$ drift.

The drift associated with $\omega_o = 0.1$ cm s^{-1} varies more among the different friction velocities than with the lighter sediment (Figure 22 and Table 6). The magnitude of the ϵ_{ust} drift is double the ϵ_{tke} drift and triple the ϵ_{cd} drift. Similar to the lighter sediment, shear shape has practically no impact on the average drift.

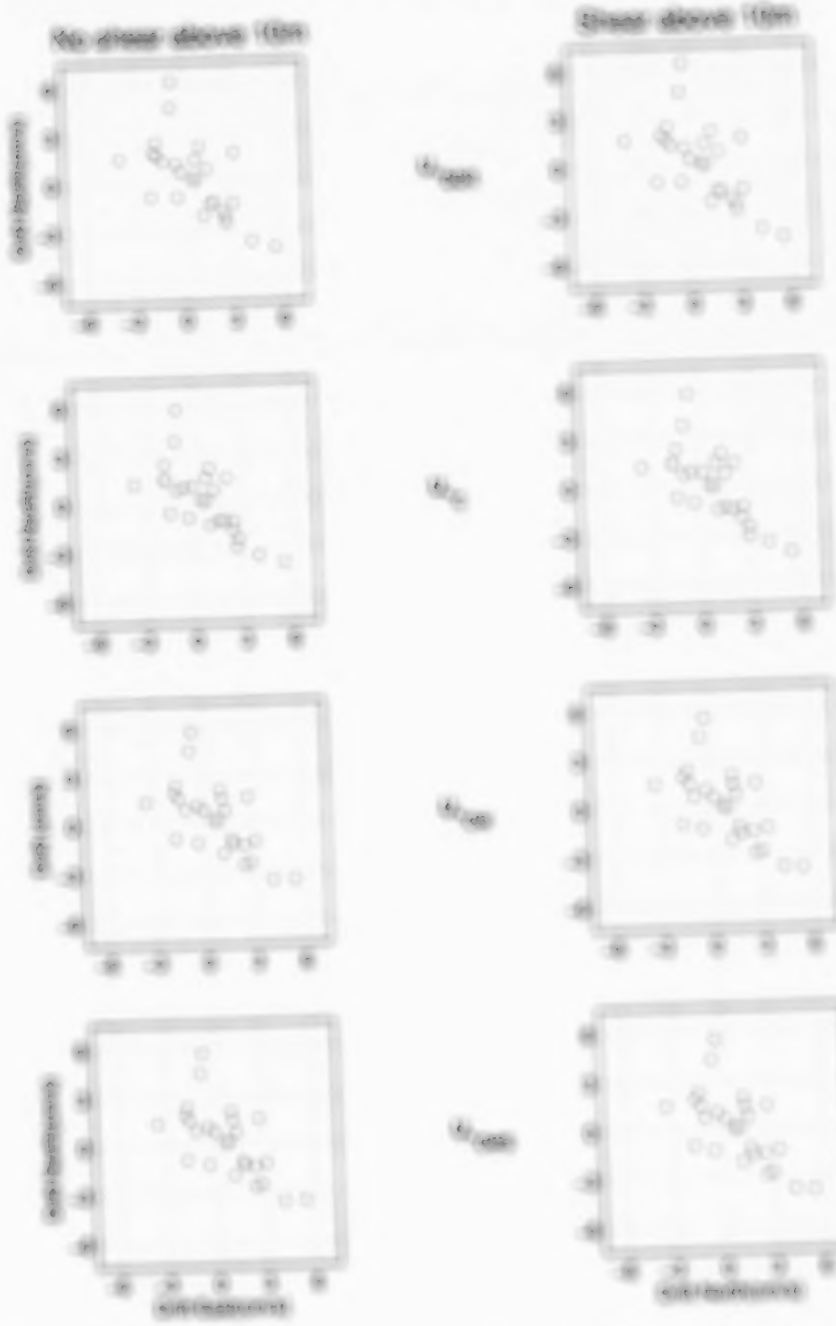

Figure 3: Velocity of the horizontal cross of cross of the sediment for the excessive resistance with the lighter sediment ($\alpha_s = 0.1$ cm s^{-1}). The + sign indicates the location of the average. All particles were released at the origin.

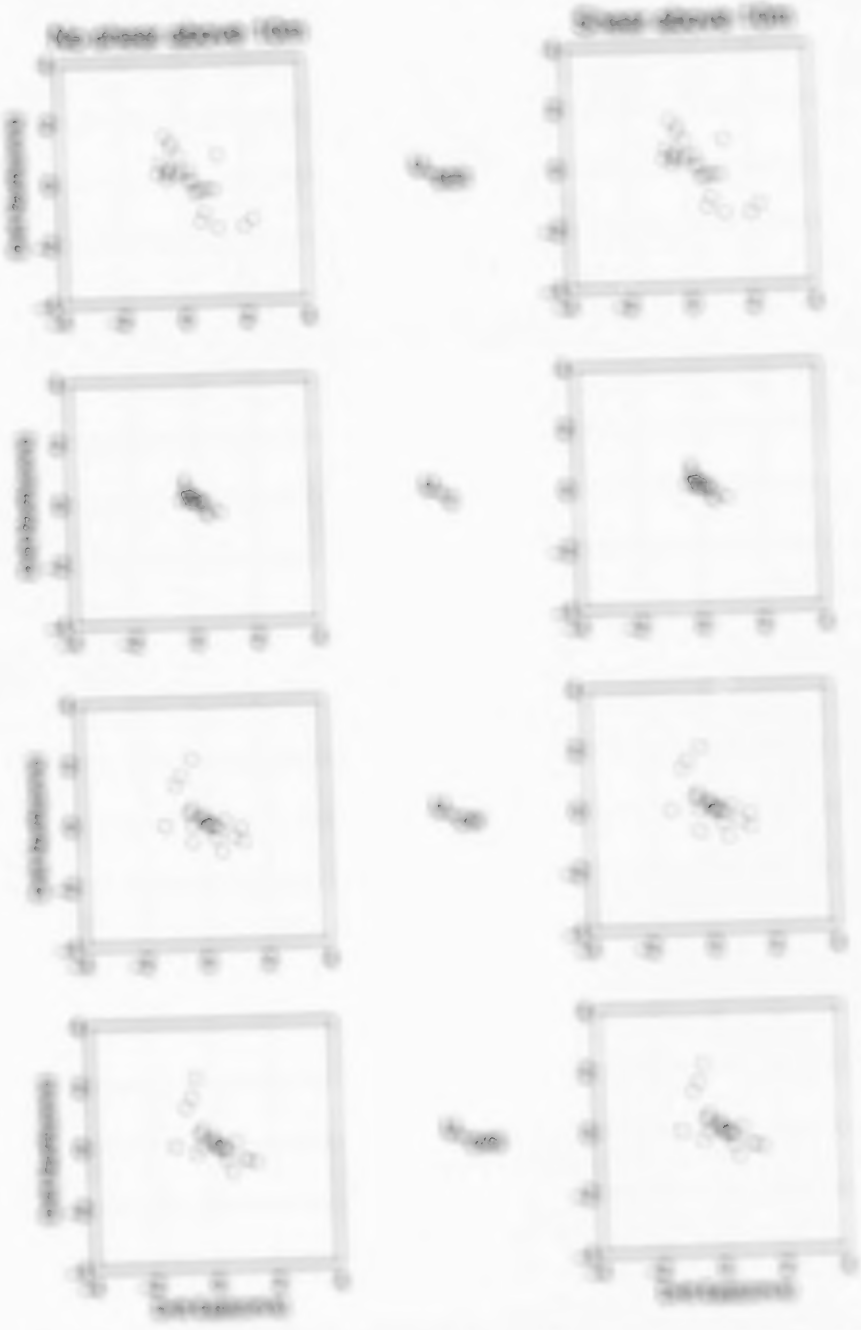

Figure 20. Velocity of the horizontal wave of wave for the ocean ascended with the wave solitary (v_x = 0.0 m s^{-1}). The = was between the source of the wave. All periods were ascended at the origin.

Table 6: The sensitivity of the mean drift to shear above 10 m. Each drift quoted is the mean over the 24 simulations; the $\pm$ is Figure 21. The units of drift are m s^{-1}.

Settling Velocity	$w_s = 0.1$ cm s^{-1}		$w_s = 0.5$ cm s^{-1}	
Shear above 10m	None	$\pm$ decay	None	$\pm$ decay
u_{tid}	0.030	0.031	0.010	0.011
u_{lin}	0.027	0.028	0.004	0.004
u_{wav}	0.029	0.029	0.008	0.008
u_{wav+}	0.029	0.029	0.008	0.008

Table 7: The sensitivity of the diffusivity to shear above 10 m. Each diffusivity is the average over the 24 simulations. The units for diffusivity are m^2 s^{-1}.

Settling Velocity	$w_s = 0.1$ cm s^{-1}		$w_s = 0.5$ cm s^{-1}	
Shear above 10m	None	$\pm$ decay	None	$\pm$ decay
u_{tid}	3.4	3.3	1.9	2.0
u_{lin}	3.8	3.4	0.5	0.5
u_{wav}	3.7	3.7	1.4	1.6
u_{wav+}	3.7	3.9	1.5	1.6

Horizontal Dispersion

The 1 day averaged horizontal diffusivity (D) is summarized in Table 7 and plotted in Figures 23 and 24. The diffusivity associated with $w_s = 0.1$ cm s^{-1} (Figure 23) has similar periodicity to u_{lin} (Figure 20). In the cases without shear above 10m, D is the lowest for u_{tid} and nearly identical for u_{lin}, u_{wav} and u_{wav+}. In the case of u_{tid}, the stronger bottom velocity suspends sediment higher in the water column where there is less shear (du_x/dz) and therefore less dispersion. Recall that the diffusivity is proportional to the mean shear experienced by the particles as they move around. Spending time in the low shear regions reduces the mean shear experienced by the particles (Hannah et al. 1995, Fischer et al. 1979). In the cases with shear above 10m, the u_{lin} diffusivity is more similar to that of u_{tid}, despite the fact that u_{lin} tends to be more similar to u_{wav} in magnitude. The source of this discrepancy has not been identified.

The scenarios with $w_s = 0.5$ cm s^{-1} (Figure 24) do not exhibit the apparent periodicity which occurred with the lighter sediment, but they do show diffusivity increasing with u_x such that $D_{tid} > D_{lin} > D_{lin-}$. The difference in the diffusion between the scenarios with and without shear above 10m is less apparent than in the lighter sediment cases. This is a consequence of the concentration profile of the heavier sediment rarely appearing above 10 m as indicated in Table 5.

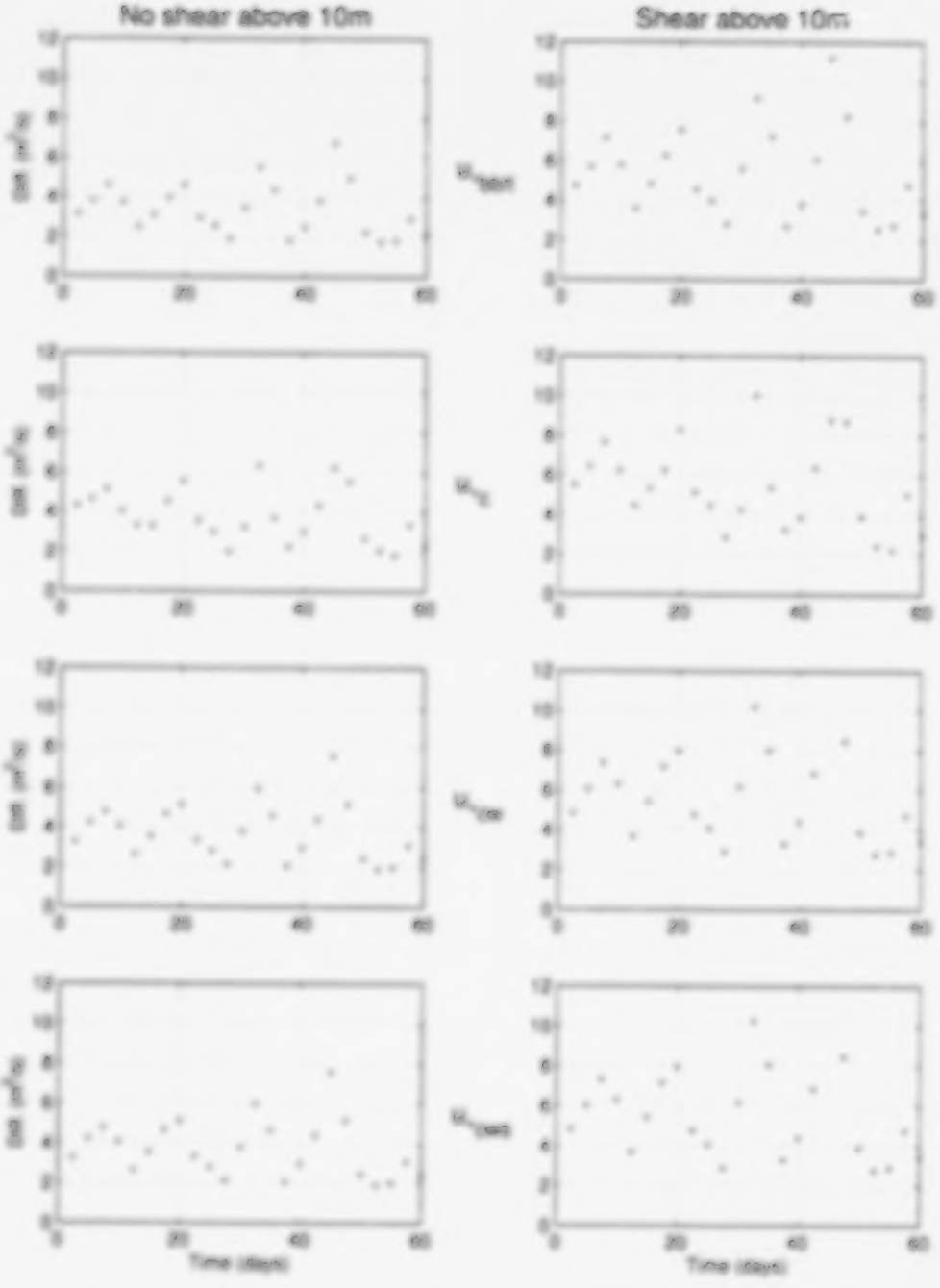

Figure 23: Five day averaged horizontal diffusivity of the sediment patch for the scenarios associated with the lighter sediment ($w_s = 0.1$ cm s^{-1}).

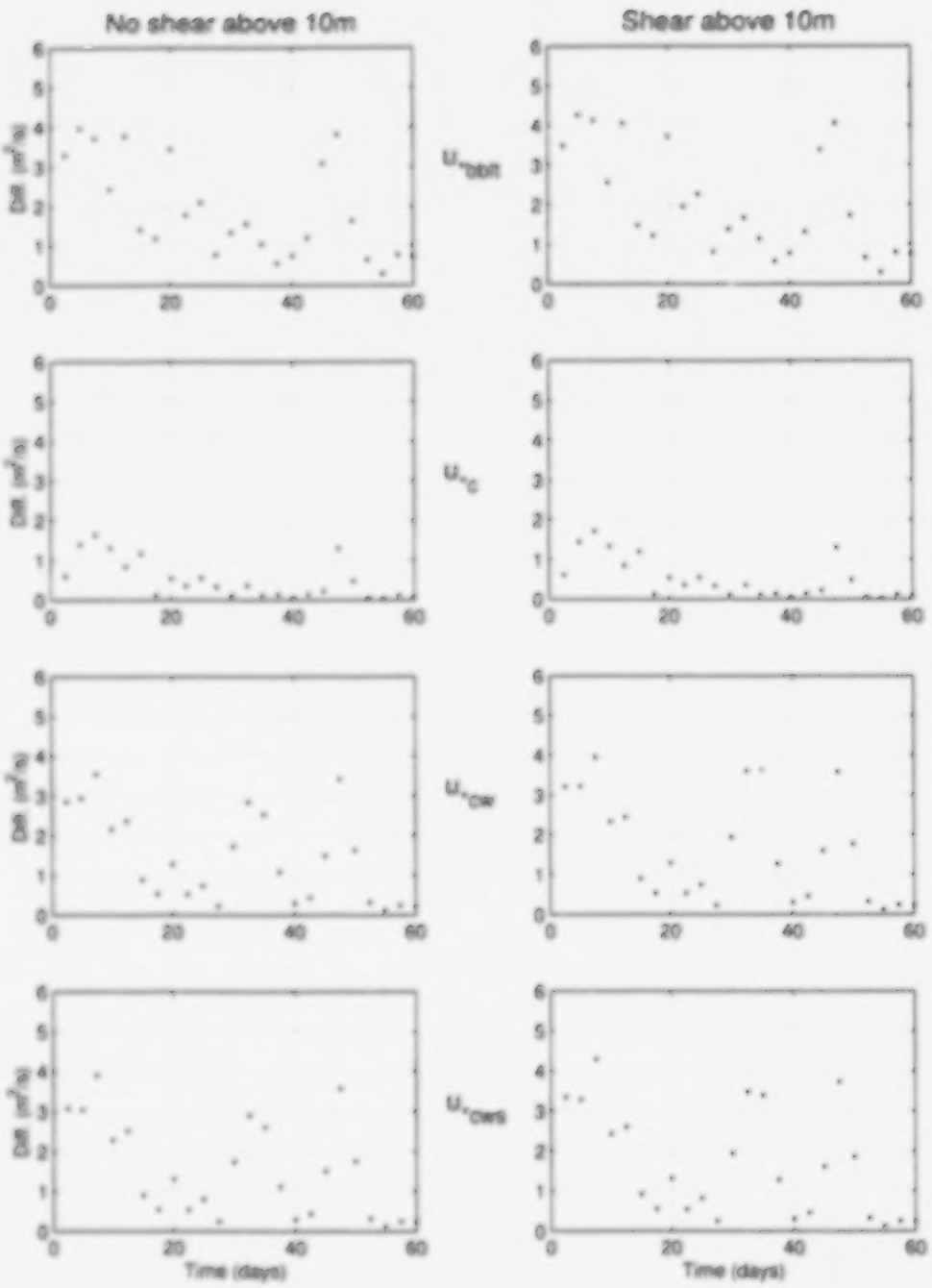

Figure 24: Overall horizontal diffusivity of the sediment patch for the scenarios associated with the heavier sediment ($w_s = 0.5$ cm s^{-1}).

6 Drift and Dispersion at Hibernia

In this section a general description of drift and dispersion at Hibernia is established. This includes a characterization of the near-bottom sediment concentration for each of the three settling velocity scenarios discussed in Section 2. The description is done first for the two fixed settling velocity scenarios and then for the variable settling velocity.

The period of the analysis is February 20, 1998 (1998 day 50) to May 14,2000 (1998 day 864). The simulations follow the pattern established in Section 5. A series of 5-day simulations are started every 2.5 days, for a total of 325 runs. The initial mass of material is 20 metric tonnes. The total currents and waves friction velocity (u_{*cw}) was used for all the simulations. The velocity extrapolation above 10 m was done using an e-folding scale of 10 m.

Both the h_{max} = 20 m and the variable h_{max} scenarios were considered, however most figures show only the variable case. Both cases are summarized in the tables. Some results with the alternative variable h_{max} (Figure 14) are included in Appendix A. Aside from some minor differences, the two versions of variable h_{max} yield the same results.

6.1 Fixed Settling Velocity

Drift

The 5 day average drift rates, with variable h_{max}, are shown in Figure 25 and 26. The drift is generally to the northwest and southeast, although there can be drift in other directions, consistent with the progressive vector diagrams from the currents (Figure 5). The drift is generally greater for the lighter sediment. Figure 25 also indicates that the 5 day drift rates are generally event driven. A strong seasonal cycle in the drift is not evident in the two years of data. For example there is rapid drift in June and July of 1998 but weak drift in June and July 1999.

The monthly averages for the slow settling velocity (w_s = 0.1 cm s^{-1}) are tabulated in Table 8. For h_{max} = 20 m, the largest monthly mean vector average drift rates are in June, July and December. There is a seasonal cycle in the mean magnitude with maxima in the summer (June and July) and the fall and early winter (October through January). The standard deviations of the drift magnitudes are generally smaller than the mean magnitudes and larger than the vector averages, indicating high variability. There are differences between the cases with h_{max} = 20 m and those with h_{max} variable, but the general patterns are similar.

The monthly drift averages for the fast settling velocity (w_s = 0.5 cm s^{-1}) are tabulated in Table 9. The overall pattern is similar to the slower settling velocity, but with smaller drift rates.

Figure 27 shows the probability that the center of mass is in a particular sector after 5 days of simulation (the distance is simply the average velocity from Figure 26 multiplied by 5 days). It shows the predominance of NW/SE drift. However, there is some probability for drift in all directions near the rig.

The south-eastward reversals are more prominent in the upper currents and therefore have greater impact on the drift of the lighter sediment than the heavier sediment. This may be why the ratio of the mean velocity (vector-averaged drift) to the mean speed (the average of the drift magnitude) is lower for the lighter sediment than for the heavy sediment ($0.69/3.1 < 0.26/0.8$ in the case of variable h_{max}, see Tables 8 and 9).

Dispersion

The overall horizontal diffusivity (D) is plotted in Figures 28 and 29 for the two fixed settling velocities ($w_s = 0.1, 0.5$ cm s^{-1}) with variable h_{max}. The climatology is summarized in Tables 10 and 11. There is a seasonal cycle in diffusivity with lower values occurring March to August and higher ones for the rest of the year peaking in December and January. This cycle is observed for both the heavier and lighter sediment.

For $w_s = 0.1$ cm s^{-1}, the monthly mean diffusivities are in the range 2.4-5.4 m^2 s^{-1}, and for $w_s = 0.5$ cm s^{-1} they are in the range 0.3-2.0 m^2 s^{-1}. From Figure 16, we know that except for a few events, the heavier sediment is generally very close to the bottom. Given that the dispersion is driven by the velocity shear, we conclude that the shear between the 3 mab and 10 mab current meters is very important to the dispersion for $w_s = 0.1$ cm s^{-1}.

Near Bottom Concentrations

The strong relationship between the near-bottom concentration and the scaling factor derived in Section 3.3 is shown in Figure 30. The correction for the vertical structure clearly captures the influence of both the differences in settling velocity and friction velocity. The result from a previous Georges Bank simulation (Loder et al., 1998) also fits the scaling argument. The slight upward curvature at the higher concentrations is a consequence of the sediment not yet having a uniform distribution across the 200 m radius sampling cylinder in some simulations.

To characterize a typical near-bottom concentration time series for each fixed settling velocity scenario, we constructed a time series using the median operator. At each time step relative to the start of the 5-day simulation, the median value of all 325 runs was selected. The two typical time series for the near-bottom concentration following the center of mass are shown in Figure 31. The concentrations are approximately 2 orders of magnitude greater than those predicted for Georges Bank by Gordon et al.

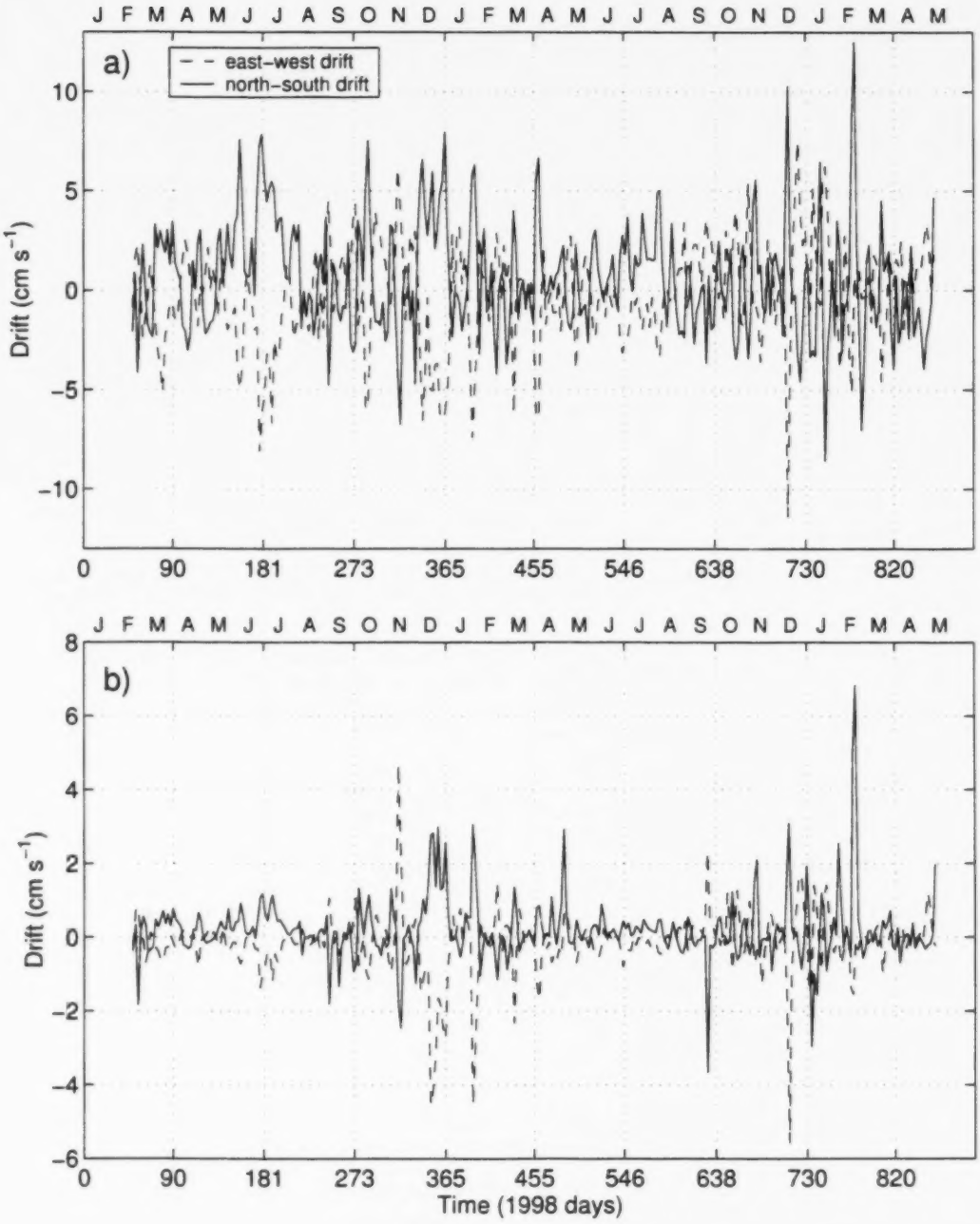

Figure 25: Five day averaged drift for a) $w_s = 0.1$ cm s^{-1} and b) $w_s = 0.5$ cm s^{-1}. h_{max} is variable.

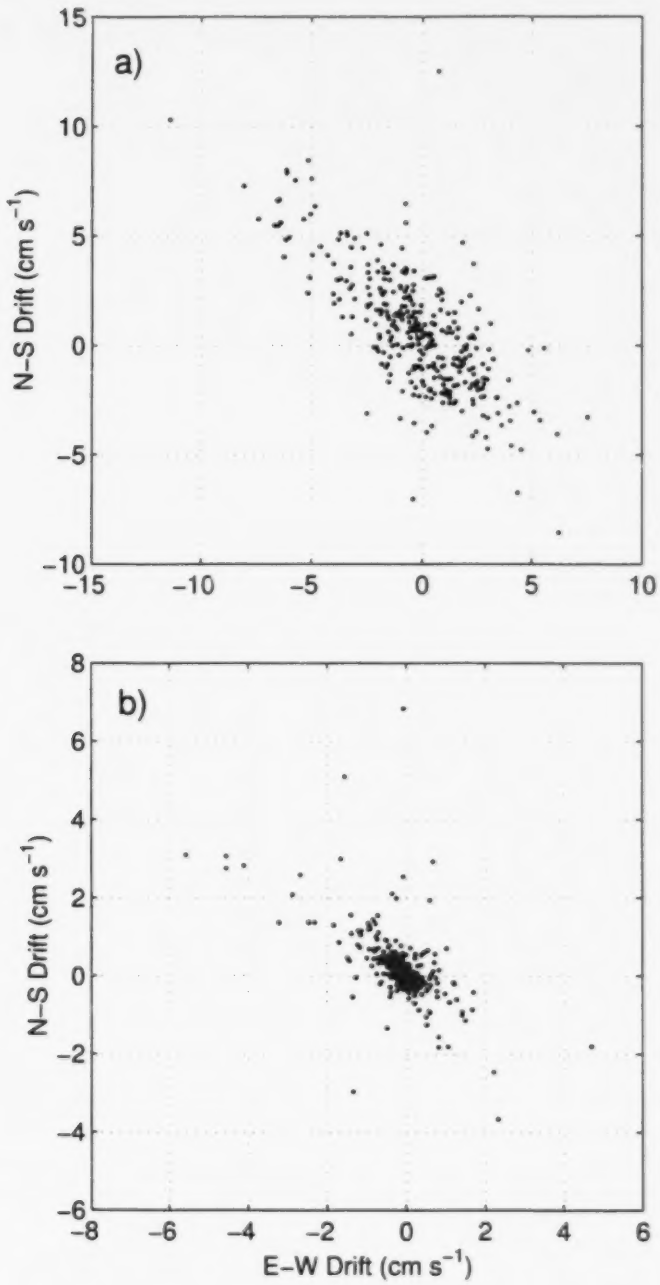

Figure 26: Five day averaged drift for a) $w_s = 0.1$ cm s^{-1} and b) $w_s = 0.5$ cm s^{-1}. h_{max} is variable. 1 cm s^{-1} is equal to 4.3 km over 5 days.

Table 8: Drift climatology of the lighter sediment.

h_{max} = 20m, velocity units are cm s^{-1}					
	Vector Average		Magnitude		
Month	Magn.	Dir (°)	Mean	Std.Dev.	Minimum
Jan	0.41	34	3.3	2.2	0.84
Feb	0.58	307	2.8	2.3	0.31
Mar	0.81	307	2.4	1.5	0.39
Apr	0.56	311	2.3	1.7	0.56
May	0.25	40	2.2	1.2	0.36
Jun	2.84	322	3.2	3.0	0.27
Jul	3.10	326	3.3	2.2	0.46
Aug	0.80	312	2.4	1.5	0.31
Sep	1.58	114	2.4	1.4	0.41
Oct	0.77	43	3.2	2.0	0.53
Nov	0.86	96	3.0	1.8	1.15
Dec	2.84	322	5.1	3.1	0.64
All	0.82	334	2.9	2.1	0.27
h_{max} = Variable, velocity units are cm s^{-1}					
Jan	0.44	102	4.0	2.7	0.36
Feb	0.35	334	3.4	2.8	0.28
Mar	0.79	294	2.6	1.6	0.17
Apr	0.20	332	2.4	1.8	0.39
May	0.29	85	2.4	1.2	0.66
Jun	2.89	322	3.2	3.1	0.21
Jul	3.15	326	3.4	2.2	0.36
Aug	0.78	307	2.4	1.4	0.26
Sep	1.68	115	2.5	1.5	0.38
Oct	0.80	42	3.3	2.1	0.45
Nov	1.07	97	3.2	1.9	1.11
Dec	2.72	325	5.4	3.3	0.51
All	0.69	338	3.1	2.3	0.17

Table 9: Drift climatology of the heavier sediment.

h_{max} = 20m, velocity units are cm s^{-1}					
	Vector Average		Magnitude		
Month	Magn.	Dir (°)	Mean	Std.Dev.	Minimum
Jan	0.21	306	1.1	1.1	0.06
Feb	0.38	330	1.0	1.3	0.04
Mar	0.19	313	0.5	0.4	0.05
Apr	0.29	313	0.5	0.5	0.05
May	0.15	8	0.4	0.4	0.03
Jun	0.47	320	0.5	0.5	0.04
Jul	0.45	321	0.5	0.4	0.09
Aug	0.07	293	0.3	0.2	0.02
Sep	0.40	141	0.7	0.9	0.06
Oct	0.18	11	0.7	0.5	0.07
Nov	0.17	103	1.0	1.0	0.03
Dec	1.37	311	1.9	1.7	0.21
All	0.26	320	0.7	0.9	0.02
h_{max} = Variable, velocity units are cm s^{-1}					
Jan	0.24	295	1.2	1.3	0.06
Feb	0.42	346	1.1	1.6	0.04
Mar	0.20	312	0.5	0.4	0.05
Apr	0.29	318	0.6	0.6	0.05
May	0.16	13	0.4	0.4	0.03
Jun	0.48	319	0.5	0.5	0.04
Jul	0.45	321	0.5	0.4	0.09
Aug	0.07	293	0.3	0.2	0.02
Sep	0.41	141	0.7	0.9	0.06
Oct	0.18	9	0.7	0.5	0.07
Nov	0.21	102	1.0	1.1	0.04
Dec	1.38	312	2.0	1.7	0.21
All	0.26	323	0.8	1.0	0.02

Table 10: Diffusivity climatology of the lighter sediment based on five day averages.

A_{max} = 20m, diffusivity units are $m^2 s^{-1}$.						
	Mean			std.dev.		Minimum
Month	K_{min}	K_{maj}	Angle (°)	D	D	D
Jan	3.3	5.7	-6	4.3	2.4	1.09
Feb	2.3	3.7	10	2.9	2.2	0.57
Mar	1.1	1.7	11	1.4	0.5	0.51
Apr	1.3	2.0	-1	1.6	0.6	0.75
May	1.4	2.0	-9	1.6	0.5	0.99
Jun	1.5	2.2	-14	1.8	0.4	1.11
Jul	1.8	2.3	-18	2.0	0.5	0.61
Aug	1.4	2.1	-18	1.7	0.4	1.03
Sep	1.8	2.5	-9	2.1	1.1	0.99
Oct	2.7	3.6	-6	3.1	2.3	0.90
Nov	3.4	4.7	-13	4.0	3.1	0.88
Dec	3.2	5.2	5	4.0	2.2	1.50
All	2.0	3.0	-5	2.5	1.9	0.51
A_{max} = Variable, diffusivity units are $m^2 s^{-1}$.						
Jan	4.5	7.7	-4	5.8	3.2	1.41
Feb	3.0	4.8	11	3.7	2.6	0.69
Mar	1.3	2.2	17	1.7	0.8	0.53
Apr	1.5	2.6	5	1.9	0.9	0.61
May	1.7	2.5	-6	2.0	0.7	1.09
Jun	1.5	2.0	-7	1.7	0.4	1.07
Jul	1.7	2.2	-16	1.9	0.5	0.64
Aug	1.5	2.1	-20	1.7	0.5	0.96
Sep	1.8	2.4	-6	2.1	1.0	0.96
Oct	2.3	3.1	-3	2.7	1.8	0.82
Nov	2.8	4.0	-11	3.3	2.1	0.87
Dec	3.6	6.2	7	4.7	2.8	1.48
All	2.2	3.4	-2	2.7	2.1	0.53

Table 11: Diffusivity climatology of the heavier sediment based on five day averages.

h_{max} = 20m, diffusivity units are m^2s^{-1}						
	Mean			std.dev.		Minimum
Month	$\bar{K}_{min}$	$\bar{K}_{maj}$	Angle (°)	D	D	D
Jan	0.9	2.0	1	1.3	1.4	0.08
Feb	0.9	1.9	-2	1.3	1.7	0.15
Mar	0.3	0.7	-15	0.4	0.2	0.09
Apr	0.3	0.9	-15	0.5	0.4	0.04
May	0.3	0.7	-3	0.4	0.5	0.03
Jun	0.2	0.7	-11	0.4	0.3	0.09
Jul	0.2	0.6	-23	0.4	0.3	0.02
Aug	0.2	0.4	-14	0.3	0.2	0.05
Sep	0.9	1.8	-19	1.2	2.0	0.07
Oct	0.8	1.0	-24	1.2	1.1	0.10
Nov	1.0	1.9	-17	1.4	1.2	0.23
Dec	1.2	3.0	-16	1.6	1.6	0.12
All	0.6	1.3	-13	0.8	1.2	0.02
h_{max} = Variable, diffusivity units are m^2s^{-1}.						
Jan	1.2	2.6	-1	1.7	1.8	0.09
Feb	1.2	2.7	-3	1.7	2.5	0.23
Mar	0.3	0.8	-14	0.5	0.3	0.09
Apr	0.4	1.0	-9	0.6	0.5	0.04
May	0.3	0.7	-3	0.5	0.6	0.03
Jun	0.2	0.7	-10	0.4	0.3	0.09
Jul	0.2	0.6	-23	0.4	0.4	0.02
Aug	0.2	0.4	-14	0.3	0.2	0.05
Sep	0.9	1.8	-20	1.2	1.9	0.07
Oct	0.7	1.0	-24	1.1	1.0	0.10
Nov	0.9	1.9	-15	1.3	1.1	0.22
Dec	1.4	3.3	-16	2.1	2.2	0.12
All	0.6	1.3	-13	0.9	1.4	0.02

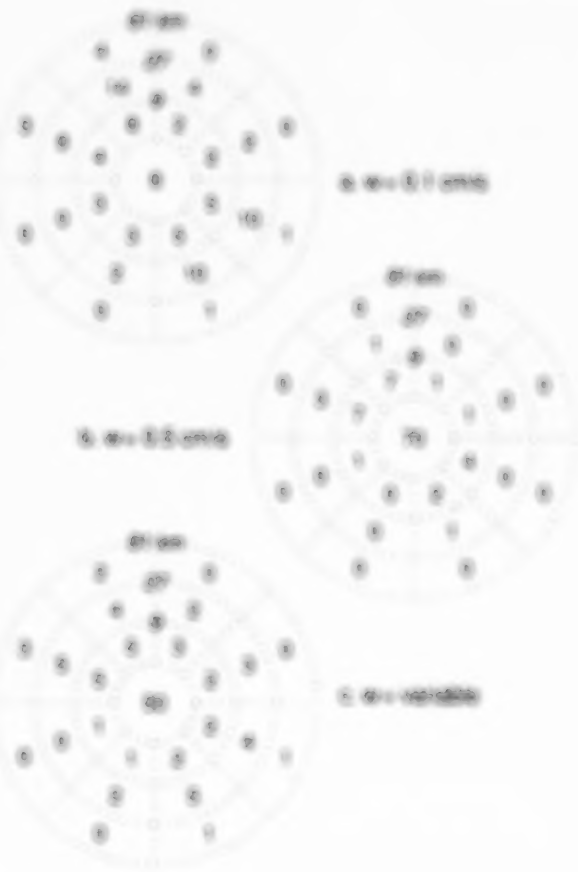

Figure 27: Maps of the probability (%) that the horizontal center of mass was in a particular sector after 5 days of simulation. The release point is the origin and the distance axis is quasi-logarithmic with intervals at 5, 9, 27, and 81 km. a) $w = 0.1$ cm s^{-1}; b) $w = 0.5$ cm s^{-1}; c) $w =$ variable. h_{max} is variable. Note that these are not probabilities per unit area.

(2000). The higher concentrations can be attributed to the smaller tidal currents at Wilmette compared to Georges Bank and the lower friction velocity associated with using SED/TRANS86 rather than the MIX drag law as was the case for the Georges Bank simulations.

Typical Sediment Distribution

The above results and analyses provide the information required to illustrate a typical sediment distribution 5 days after the discharge of sediment to the bottom boundary

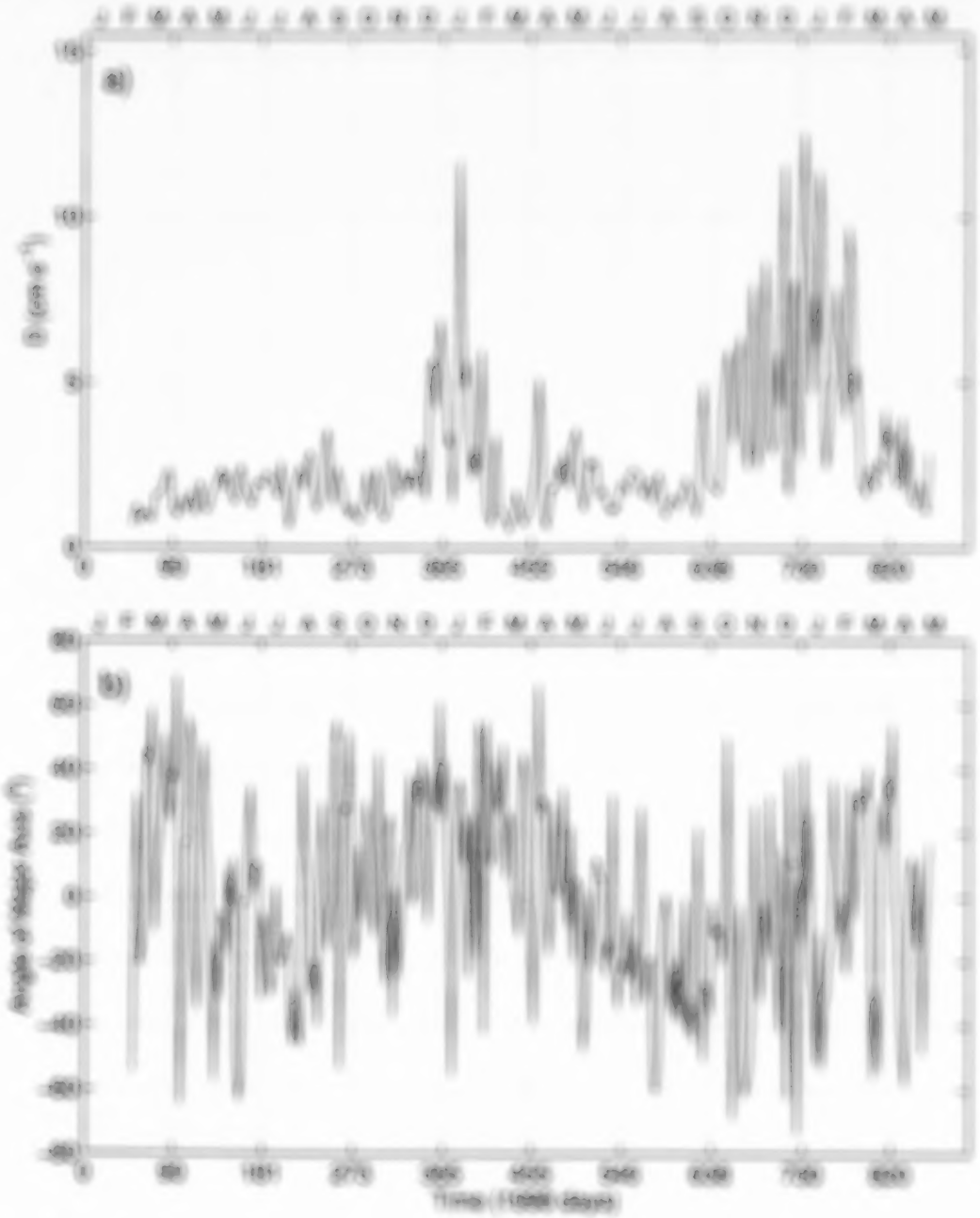

Figure 36: Five day averaged diffusion of the lighter sediment. (a) overall magnitude, (b) angle of major axis from north. K_{max} is variable.

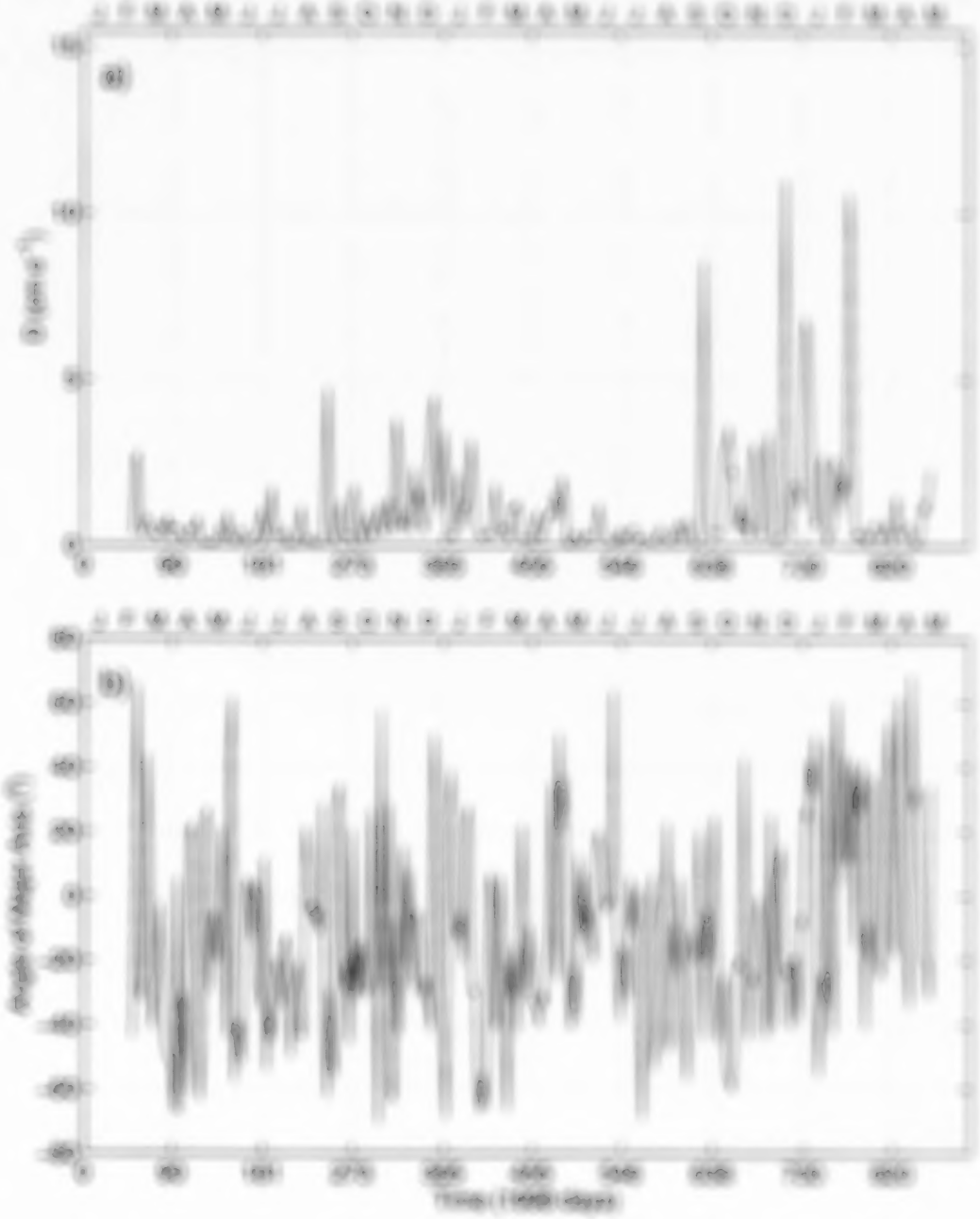

Figure 30: Five day averaged diffusion of ice tracer ordinate. (a) overall magnitude. (b) angle of major axis from north. θ_{max} is variable.

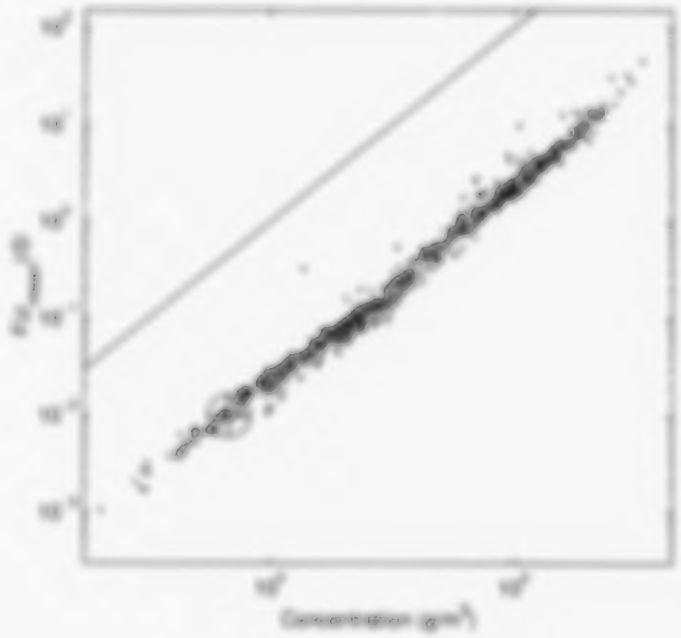

Figure 39. The scaling factor for near-bottom concentration (C_s) versus the near-bottom concentration following the horizontal center of mass. The near-bottom concentration was averaged over the last 12 hours of a five day run using a cylinder of radius 200 m and height of 10 cm. Results for both w_s = 0.1 and 0.5 cm s^{-1} are included. h_{max} = 30 m. The ⊕ indicates a Mid application on Georges Bank (Loder et al., 1998). The straight line represents a 1:1 relationship.

layer (Figure 32). The typical drift direction and magnitude were taken from Tables 6 and 9 for runs performed with variable h_{max}. The drift magnitude was taken as equal to the mean magnitude and a drift direction as equal to the vector averaged direction. The diffusivities K_{max}, K_{min} and Angle from Tables 10 and 11 were used to define the shape and orientation of the sediment patch. The ratio of local concentration to the concentration at the center of mass (maximum concentration) is represented by contours for 0.5, 0.1 and 0.01. The maximum concentrations after 5 days were taken from the average concentration curves shown in Figure 31 which were based on a calculation using the bulk release of 20 x 10^9 kg of sediment. The typical patch parameters discussed above are summarized in Table 12.

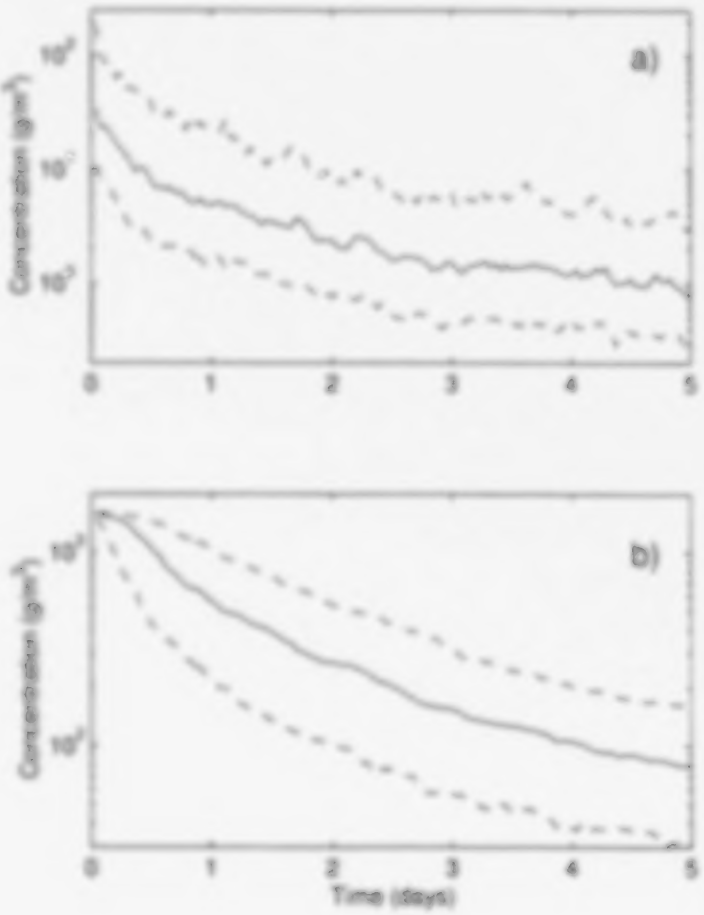

Figure 31: Time series of median near bottom concentration at the horizontal center of mass for (a) w_s=0.1 cm s^{-1} and (b) w_s=0.5 cm s^{-1}. A_{max} is variable. The upper and lower dashed lines are the 75 and 25 percentiles respectively. At each time the median is constructed by considering all 325 simulations.

6.2 Variable Settling Velocity

To understand how the variable settling velocity affects the likelihood of high concentration events we consider the probability that the mean concentration at the center of mass over the last day (day 5) exceeds a certain level (Figure 33). For w_s = 0.1 cm s^{-1} there is a 50% probability that the mean concentration over the last day exceeds 2.0 g m^{-3}, for w_s = 0.5 cm s^{-1} it is 100 g m^{-3} and 30 g m^{-3} for the variable settling velocity. Tedford et al. (2002) reported on a preliminary version of these calculations. Their version of

Table 12: Summary of typical sediment patch characteristics.

Settling Velocity		$w_s = 0.1$ cm s^{-1}	$w_s = 0.5$ cm s^{-1}
Drift	Magnitude (cm s^{-1})	3.1	0.8
	Direction	-22°	-37°
Diffusion	Minor axis (m^2/s)	2.2	0.6
	Major axis (m^2/s)	3.4	1.5
	Angle of axis	-2°	-13°
Concentration	C_{max}	0.8	78
(g/m^3)	CR=0.5	0.4	39
	CR=0.1	0.08	7.8
	CR=0.01	0.01	0.78

Table 13: Horizontal diffusivity quartiles for the three settling velocity scenarios.

	Diffusivity (m^2 s^{-1})		
w_s (cm s^{-1})	25%	50%	75%
0.1	1.41	2.00	3.05
0.5	0.23	0.46	1.06
Variable	0.24	0.64	1.85

Figure 33 had higher concentrations for the $w_s = 0.5$ cm s^{-1} and variable cases. This was due to an error in the temporal interpolation of the friction velocity in `bblt` when the friction velocity was computed using SEDTRANS96. The error does not affect the conclusions in Tedford et al. (2002) and was corrected for this report.

The concentrations from the variable settling velocity scenario are identical to those of the fast settling velocity for the highest 20% of the concentrations and approach the values of the slow settling velocity for the lowest 20% of the concentrations. There is a rapid transition between high and low concentrations at about the 50% level. The highest 20% did not experience breakup and are identical to the fast settling velocity simulations. The lowest 20%, with concentrations less than the minimum from the fast settling velocity simulations, did experience breakup. In the transition region there is an equal mix of simulations which did and did not experience breakup stress. This was determined by checking the settling velocity at the end of each run.

Similarly, the drift of the variable w_s runs (Figure 27c) is a mixture of the two fixed w_s cases. The drift is within 3 km of the release point 50% of the time (like w_s =0.5 cm s^{-1}) and beyond 9 km 32% of the time (like w_s =0.1 cm s^{-1}).

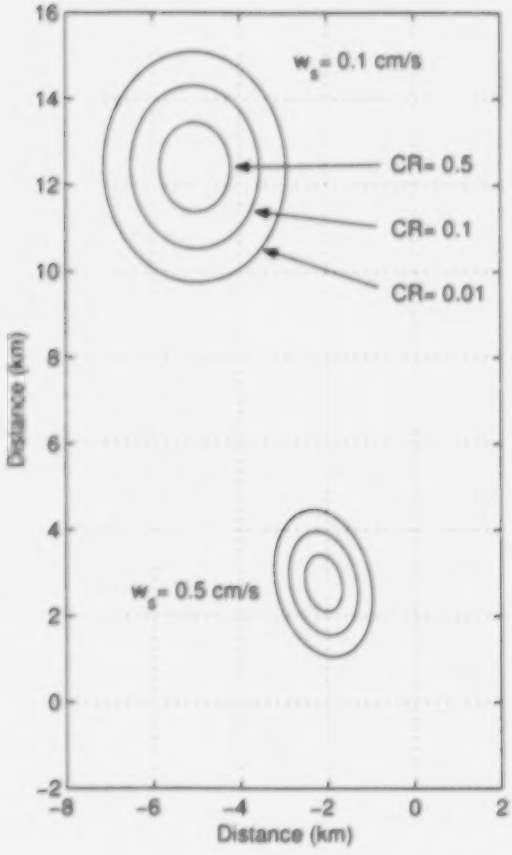

Figure 32: Typical horizontal sediment distribution and drift after 5 days. CR is the ratio of the concentration at the indicated ellipse to the concentration at the center (maximum). h_{max} is variable.

The diffusion statistics shown in Table 13 also indicate that the results of the variable settling velocity runs fall in between those from the fast and slow settling velocity. A notable feature is that the median (50%) of the variable runs is much closer to the median of the faster settling velocity runs than to the slower ones.

A useful statistic for interpreting the variable settling velocity results is the likelihood that a specified period of time will be exceeded before a u_*^c event occurs or conversely the likelihood that u_* will exceed u_*^c at least once over a specified time interval. Figure 34a shows that from an arbitrary starting time, the probability that u_* will exceed 1 cm s^{-1} at least once during the next 5 days is close to 50%. The probability that breakup will occur during the first day of a simulation is about 20%, which is consistent with the concentrations from the variable settling velocity simulations approaching those from the slow settling velocity for the lowest 20% of the concentrations (Figure 33).

Figure 34a also illustrates the sensitivity of the breakup probability to the choice of u_*^c. At five days a 25% increase in u_*^c reduces the probability from 50% to 30% and a 25% decrease in u_*^c increases the probability to 90%. Thus uncertainties in u_*^c of the order of

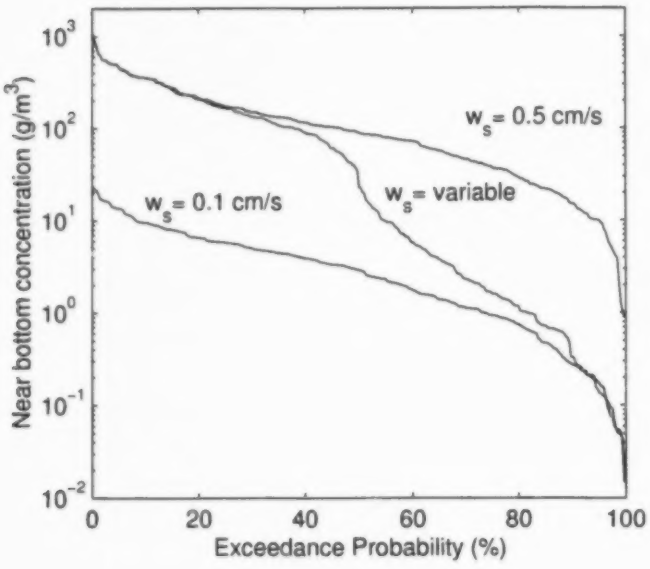

Figure 33: The probability that the mean concentration over the last day exceeds a given concentration.

25% have a large impact on the expectation of a floc breakup event on time scales of days to months. Hill et al. (2001) report that all the flocs are gone when the stress exceeds 0.1 Pa, however it is possible that the flocs start breaking up at lower stress and that the breakup process is better represented as an increasing probability of breakup over a (possibly narrow) range of bottom stress.

Figure 34b shows a breakup exceedence curve for each of the four seasons. In the fall and winter, the probability that the time will exceed five days before a u_*^c event is approximately 75%, substantially greater than in the spring and summer when the exceedence probability is near 30%. The difference in these curves can be attributed to the larger waves during the fall and winter compared to the spring and summer.

7 Discussion and Summary

During a field program covering the period from February 1998 to June 2000 waves, near bottom current data were collected near the Hibernia oil production platform. The long term drift at the site is to the northwest with occasional reversals to the southeast. The reversals are more pronounced in the currents at 10 mab than at 3 mab. There was no obvious seasonality in the magnitude or direction of the currents. Wave observations show strong seasonality with larger waves occurring in fall and early winter. The CTD

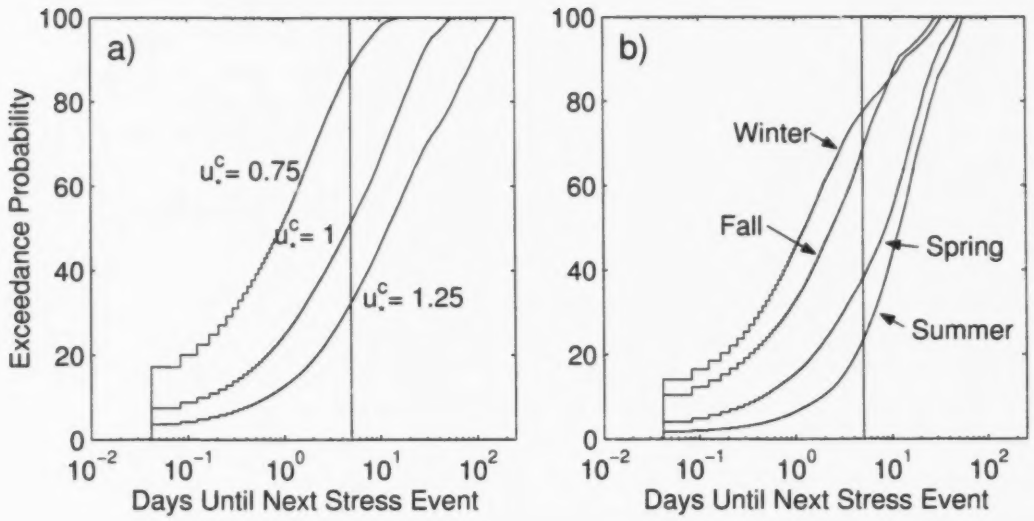

Figure 34: The probability that the period of time until the next u_*^c event will exceed X days. a) Three different values of u_*^c (cm s^{-1}); b) Seasonal differences in exceedance probability for u_*^c=1 cm s^{-1}. The vertical line is at 5 days.

taken during the period of the study show a stratified water column from late spring until the end of fall (last available observation).

The current reversals illustrate some of the limitations of the modelling with currents at only one horizontal location. In particular, there is always the issue of whether the observed variability is solely due to temporal variability or whether spatial structure in the currents are important. One interpretation of the current reversals is that it reflects the presence of a sloped horizontal gradient (front) in density and currents that occasionally impact the mooring. Such a front leads to two problems. The first is the implicit assumption that nearby currents are highly correlated with the measured ones. A front crossing the mooring location can render this assumption invalid. The likely consequences are incorrect estimates of the direction of mean drift and underestimated diffusivity due to the neglect of the horizontal shears. The second problem is the potential for a strong density gradient between the 3 and 10 mab observations correlated with the large velocity shears. Such a gradient is not reflected in h_{max}. `bblt` will mix particles across such a density gradient which will result in large diffusivity even though in reality particles were trapped below the gradient. Neither of these problems are addressed in this report.

A study of the correlation between currents as a function of horizontal separation could be conducted using coincident current data observed on the North East Grand Bank. Such a study could be conducted using the archived data in the BIO database

(`www.mar.dfo-mpo.gc.ca/science/ocean/database/data_query.html`), but is beyond the scope of this work.

The suspended sediment height showed some seasonality with sediment suspended higher in the fall and winter and lower in the spring and summer. For the slower settling velocity (marine flocs) the friction velocity was generally large enough to project the concentration profile high into the water column. As a result, the seasonal variation in the median height was primarily controlled by the seasonal variation in the stratification (h_{max}). For the faster settling particles (drill mud flocs) the median height is generally small and unaffected by the stratification. As a result the seasonal variation in the median height was controlled by the seasonal cycle in storms and waves. The median height of the faster settling particles typically approached zero during the summer months indicating negligible suspension.

The influence of shear above 10 m was investigated. In the case of the faster settling particles the two different velocity extrapolations showed negligible differences in both drift and diffusivity. The slower settling particles were sensitive to the velocity extrapolation in terms of diffusivity only, with greater diffusivity occurring in the runs with the exponential shear decay above 10 m. Both approaches to the velocity extrapolation will underestimate the shear in the upper water column especially during storms. Thus we have likely underestimated the diffusivity in the winter when the water column is unstratified and the vertical distribution related to the slow settling velocity typically extended to the surface.

The sensitivity analysis also showed how the different friction velocity calculations affect diffusivity and drift. In the case of the slower settling particles, drift was very similar for the four different friction velocities; diffusivity was on average 10 to 15% less for the runs conducted using u_{*d}. In the case of the faster settling particles drift and diffusivity were approximately doubled using u_{*d} compared to u_{*cw} and u_{*cws}.

The results of the runs covering two years indicate the drift is generally oriented along the northwest/southeast axis although the net drift after 5 days can be in any direction. The typical magnitude of the drift is 0.8 cm s^{-1} for the fast settling velocity and 3.1 cm s^{-1} for the slow settling velocity. The drift is event driven and therefore the 2 years of data are insufficient for a robust estimate of the seasonal cycle. For example June and July 1998 had several large drift events but there were almost no such events in the summer of 1999.

The five day diffusivity showed very high variability with the monthly standard deviation often exceeding the mean, highlighting the importance of events rather than tides. The diffusivity for the fast settling velocity case is typically 0.9 m^2/s with a range from almost 0 to 12 m^2/s. For the slow settling velocity the diffusivity is typically 2.7 m^2/s with a range from 0.5 to 13 m^2/s. The monthly averages are generally larger in the fall and winter than the spring and summer.

The experiments with the stress dependent settling velocity illustrated how flocculation dynamics can affect the estimate of near bottom concentration. With a floc breakup stress of 0.1 Pa, the new formulation did not affect the magnitude or frequency of the high concentration events because only 50% of the simulations experienced breakup during their 5 day simulation period. Since high stress is generally associated with low near-bottom concentrations in these simulations, the effect of floc breakup was to reduce the near bottom concentrations in the simulations with low and intermediate concentrations. The frequency of breakup events was sensitive to the choice of breakup stress. A useful statistic for interpreting the results is the likelihood that the u_* will exceed u_*^c at least once over a specified time interval. At Hibernia the probability that u_* will exceed 1 cm s^{-1} at least once during the next 5 days is close to 50%. This means that the likelihood of observing the fast settling particles during an annual survey depends not only on sampling within the sediment patch but also on sampling within a few days of the mud discharge. We note that the choice of the stress dependent settling velocity places a premium on accurate estimates of friction velocity and break-up stress.

If one accepts the stress dependent settling velocity as a reasonable model for the settling velocity, then the initial settling velocity becomes a crucial parameter for estimating the likelihood of large near-bottom concentrations. Since flocculation is a concentration dependent process, one needs to consider the mode of discharge because that has an impact on the ambient concentration of drill mud. The mode of discharge that leads to high concentrations of drilling mud (and likely large settling velocities) is a bulk dump at the end of a section. The direct discharge to the sea floor while drilling the initial open-circuit section may also be a high concentration process that leads to large settling velocities, however the process is not well understood. Other modes of discharge into the ocean may not lead to similar settling velocities. For example, drill mud can enter the ocean stuck onto the rock cuttings that are discharged. The water-based mud is probably washed off the cuttings during the descent to the bottom. This is likely a low concentration process and the mud is probably incorporated directly into the background floc population. In addition, operating procedures such as diluting the drilling mud during discharge will lower the initial concentrations and likely result in less flocculation and smaller settling velocities. Therefore prediction of near-bottom concentrations requires knowledge of both the volume of discharge and the method of discharge.

Given the strong sensitivity of the near-bottom concentrations to the settling velocity, a partitioning of the initial drill mud mass into a range of flocs (settling velocities) will have a substantial impact on the estimated near-bottom concentration before breakup.

Which simulations are most likely to represent conditions at Hibernia during the period of the study? The two modes of discharge mostly likely to lead to large settling velocities are both associated with drilling the early stages of a new well. As the initial production well at Hibernia was drilled in 1997, at least a year before the study period, the initial settling velocity of $w_0 = 0.5$ cm s^{-1} is likely too large. The most likely scenario is that the drilling muds were rapidly incorporated into the population of background

marine flocs with $w_s \sim 0.1$ cm s^{-1}. However the flocculation dynamics of synthetic muds (SBM) and their interactions with natural flocs are not well known. Thus the possibility of larger settling velocities does exist.

In addition, the initial mass of 20 mt represents a typical bulk discharge at the end of the initial open circuit portion of several wells on the Scotian Shelf. It is unlikely that such a large volume has been discharged in such a short time at Hibernia since the initial production well was drilled in 1997. Thus the concentrations reported here are much higher than would be expected for the period of this study.

The friction velocity, drift and diffusivity are generally smallest in the summer and there are the fewest breakup events in the summer. As such one might expect that the largest concentrations would be found at Hibernia in the summer. However summer is also the time of the greatest surface stratification. Therefore near-surface or mid-depth discharges of drilling mud in the summer may not reach the sea floor.

Acknowledgements We are grateful to the (Canadian) Federal Panel for Energy, Research and Development (PERD) for funding. Support was provided from the Offshore Environmental Impact POL (model development and application) and the Offshore Environmental Factors POL (support for the field study). We also thank Yuri Geshelin, John Loder and Kee Muschenheim for the current meter data, Carl Anderson for the bottom stress calculations, and Tim Milligan for encouraging us to develop the stress dependent settling velocity. In addition, we thank John Loder and Brian Petrie for their reviews.

References

Anderson, C. 2001. Seabed shear stress estimates at the Cohasset and Hibernia oil production sites. Can. Data Rep. Hydrogr. Ocean Sci. 216:viii+54pp.

Csanady, G. T. *Turbulent Diffusion in the Environment.* D. Reidel Publishing Company, 1973.

H. B. Fischer, E. J. List, R. C. Y. Koh, J. Imberger, and N. H. Brooks. *Mixing in Inland and Coastal Waters.* Academic Press, 1979.

Geshelin Y. S., J. W. Loder and Kee D. Muschenheim. 2001. Moored current and hydrographic measurements at the Hibernia OGBS site. Can. Data Rep. Hydrogr. Ocean Sci. (In prep.).

Gordon Jr., D. C., P. J. Cranford, C. G. Hannah, J. W. Loder, T. M. Milligan, D. K. Muschenheim and Y. Shen. 2000. The potential effects of exploratory hydrocarbon

drilling on Georges Bank scallop populations. Can. Tech. Rep. Fish. Aquat. Sci. 2317: 116 pp.

Grant, W. D. and O. S. Madsen. 1986. The continental shelf bottom boundary layer. *Annual Review of Fluid Mechanics* **18** 265-305.

Hannah, C.G., Y. Shen, J.W. Loder and D.K. Muschenheim. 1995. **bbl**t: Formulation and Exploratory Applications of a Benthic Boundary Layer Transport Model. Can. Tech. Rep. Hydrogr. Ocean Sci. 166: vi + 52 pp.

Hill, P. S., J. P. Syvitski, E. A. Cowan and R. D. Powell. 1998. In situ observations of floc settling velocities in Glacier Bay, Alaska. *Marine Geology*, **145**: 85-94.

Hill, P. S., T. G. Milligan, and W. R. Geyer. 2000. Controls on effective settling velocity of suspended sediment in the Eel River flood plume. *Cont. Shelf Res.*, **20**: 2095-2111.

Hill, P. S., G. Voulgaris, and J. H. Trowbridge. 2001. Controls on floc size in a continental shelf bottom boundary layer. *J. Geophys. Res.*, **106**: 9543-9549.

Li, M.Z. and C. L. Amos. 2001. SEDTRANS96: the upgraded and better calibrated sediment-transport model for continental shelves. *Comput. Geosci.*, **27**: 619-645.

Loder, J.W., C. G. Hannah, Y. Shen, E. A. Gonzalez, Z. Xu. 1998. Suspended sediment drift and dispersion on Georges Bank. Unpublished manuscript with 188 pages. Many of the results were reported in Gordon et al. (2000).

Milligan, T. G. and P. S. Hill. 1998. A laboratory assessment of the relative importance of turbulence, particle composition, and concentration in limiting maximal floc size and settling behaviour. *J. Sea Research* **39**: 227-241.

Rouse, H. 1937. Modern concepts of the mechanics of turbulence. *Trans. Am. Soc. Civ. Eng.*, **102**, 463–543.

Tedford, T., Gonzalez, E., and Hannah, C.G. 2001. **bbl**t Version 3.1 User's Manual. Can. Tech. Rep. Hydrogr. Ocean Sci. 213: v + 48 pp.

Tedford, T., C. G. Hannah, T. G. Milligan, J. W. Loder, and D.K. Muschenheim. 2002. Flocculation and the fate of drill mud discharges. In: Estuarine and Coastal Modelling: Proceedings of the 7th International Conference (St. Petersburg Fl., 5-7 November, 2001). M.L. Spaulding (Editor). ASCE. 294-309 pp.

A Alternative Maximum Sediment Height Profiles

This section compares some of the plots from Section 6 to their counterparts which use the alternative maximum sediment height profile. The alternative profile used 84 m as the sea floor bottom for converting the depths of the pycnoclines in Figure 12 to heights above bottom. The differences are minor and not important for this study.

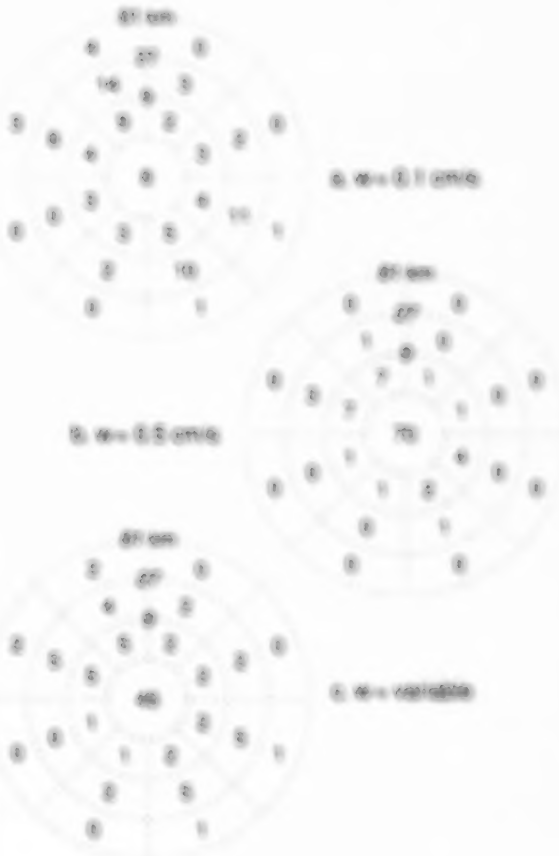

Figure 35: Maps of the probability that the horizontal center of mass was in a particular sector after 5 days of simulation. The release point is the origin and the distance axis is quasi-logarithmic with intervals at 3, 9, 27, and 81 km. a) $w = 0.1$ cm s^{-1}; b) $w = 0.5$ cm s^{-1}; c) w = variable. NOTE: uses alternative h_{max} profile.

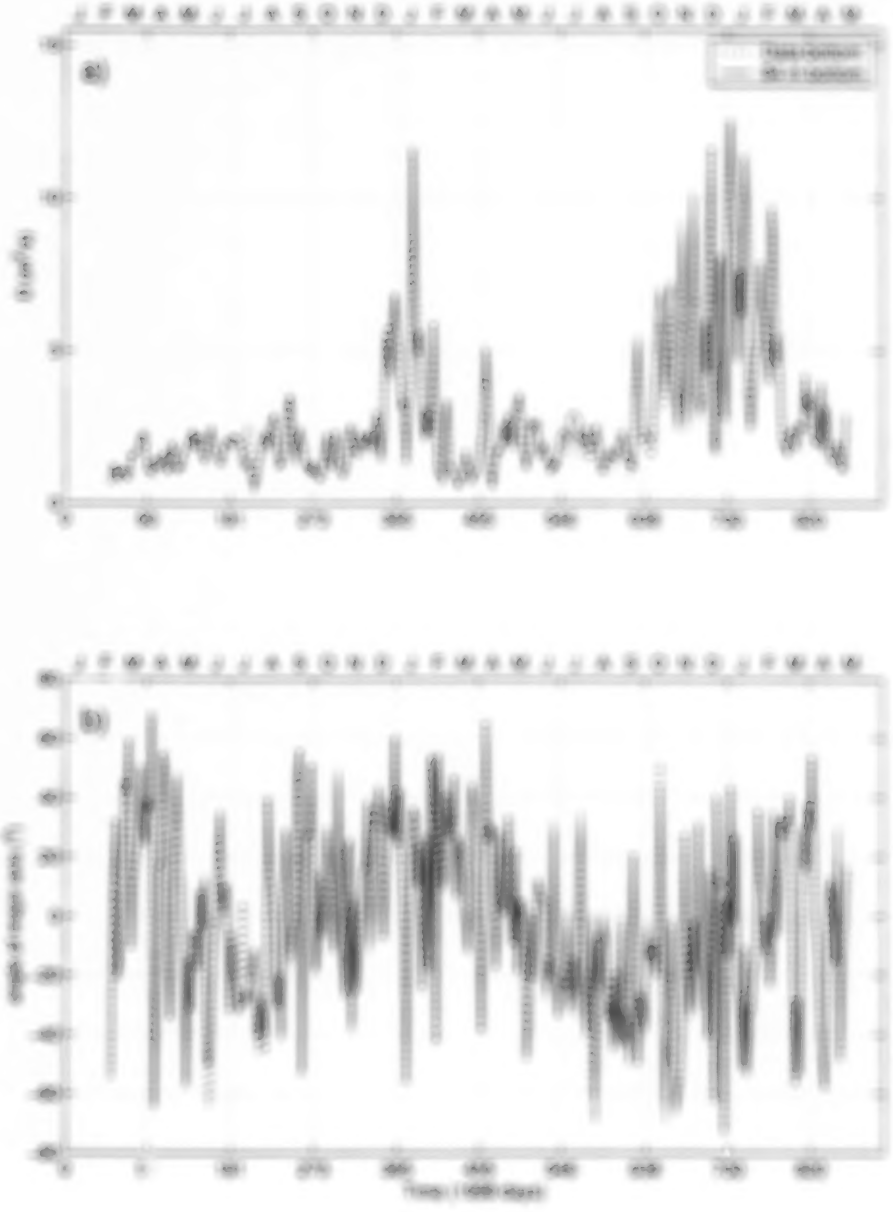

Figure 36: Five day averaged diffusion for the lighter sediment with both k_{max} profiles. a) overall magnitude, b) angle of major axis from north.